FINAL SCIENTIFIC REPORT

Organization:	The Regents of the University of California University of California, San Diego La Jolla, CA 92093
Department:	Department of Mathematics
Principal Investigator:	M. Rosenblatt
Title:	Three-dimensional bispectra and the mean rate of transfer of energy
Agency and Grant No.:	National Aeronautics and Space Agency NSG-2376
Period:	3/1/79 - 10/30/80

(NASA-CR-164217) ESTIMATING THREE-DEMENSIONAL ENERGY TRANSFER IN ISOTROPIC TURBULENCE Final Scientific Report, 1 Mar. 1979 - 30 Oct. 1980 (California Univ., San Diego, La Jolla.)

N81-22822

Unclas

G3/67 42127

Estimating three-dimensional energy transfer in isotropic turbulence

K. S. Lii
Department of Statistics
University of California, Riverside, CA 92502

K. N. Helland
Institute for Pure and Applied Physical Sciences and
Department of Applied Mechanics and Engineering Sciences
University of California, San Diego, La Jolla, CA 92093

M. Rosenblatt
Department of Mathematics
University of California, San Diego, La Jolla, CA 92093

1. Introduction

The research reported on in this paper is a continuation of that considered in previous work (Lii et al. (1976), Helland et al. (1979)). Here the attempt is to get a three-dimensional spectral view of grid-generated turbulence. This is done by setting an x-wire probe at a fixed position, and setting two single wire probes at a number of locations in the same plane perpendicular to the mean flow in the wind tunnel. The locations of the single wire probes are determined by pseudo-random numbers (Monte Carlo). Second-order spectra and cross-spectra are estimated. The assumption of isotropy relative to second-order spectra is examined. Third-order spectra are also estimated corresponding to the positions specified. A Monte Carlo Fourier transformation of the downstream bispectra corresponding to integration across the plane perpendicular to the flow is carried out assuming isotropy. Further integration is carried out over spherical energy shells. The object is to get an estimate of the spectral transfer function that indicates the rate of decay of energy.

2. Basic theoretical background

2.1 Energy transfer equations

Let $\bar{v}(\bar{x}, t) = (v_1, v_2, v_3)$ be the velocity field as a function of location $\bar{x} = (x_1, x_2, x_3)$ and time t. In the model of homogeneous turbulence, $\bar{v}(\bar{x}, t)$ is regarded as a random solution of the Navier-Stokes equation

$$\frac{\partial \bar{v}(\bar{x}, t)}{\partial t} + \bar{v} \cdot \bar{\nabla} \bar{v} = -\frac{1}{\rho} \nabla p + \nu \nabla^2 \bar{v}$$

and the continuity equation

$$\nabla \cdot \bar{v} = 0$$

that is stationary in $\bar{x}$. Here ∇ is the gradient operator, ρ is the density, p is the thermodynamic pressure, ν is the kinematic viscosity, and ∇^2 is the Laplacian. Given finiteness of second order moments, it follows that $\bar{v}(\bar{x}, t)$ has a Fourier representation

$$\bar{v}(\bar{x}, t) = \int e^{i\bar{k} \cdot \bar{x}} \, d\bar{z}(\bar{k}, t) \quad .$$

Here $\bar{k} = (k_1, k_2, k_3)$ is the wavenumber vector. Existence of appropriate moments is assumed whenever required. The spectral matrix $f(\bar{k}, t)$ is given by

$$f(\bar{k}, t) \, \delta_{\bar{k}, \bar{k}'} \, d\bar{k} = E \{ d\bar{z}(\bar{k}, t) \, d\bar{z}^{*}(\bar{k}', t) \}$$

$$= (E \{ dz_\alpha(\bar{k}, t) \, dz_\beta^{*}(\bar{k}', t) \} \; ; \quad \alpha, \beta = 1, 2, 3) \quad .$$

where the asterick is used to denote the transpose conjugate. From now on the time dependence will be implicit and the explicit appearance of t will be suppressed. The third-order moments

$$Q_{\alpha,\beta}(\bar{k},\bar{k}')\,d\bar{k}\,d\bar{k}' = \mathrm{Im}\,E\{k_\alpha dz_\alpha(\bar{k}-\bar{k}')\,dz_\beta(-\bar{k})\,dz_\beta(\bar{k}')\}\,; \quad \alpha,\beta = 1,2,3.$$

The energy associated with wave number vector $\bar{k}$ is $f_{ii}(\bar{k})$ (repeated indices are used to imply summation over $i = 1, 2, 3$).

The equation

$$\frac{\partial}{\partial t}\left(\frac{1}{2} f_{ii}(\bar{k})\right) = \int Q(\bar{k},\bar{k}')\,d\bar{k}' - \nu\,|\bar{k}|^2 f_{ii}(\bar{k})$$

relates second- and third-order spectra and describes the rate of change of energy with time.

$$Q(\bar{k},\bar{k}') = \sum_{\alpha,\beta} Q_{\alpha,\beta}(\bar{k},\bar{k}')$$

is considered to be the net mean rate of energy transfer from $d\bar{k}'$ to $d\bar{k}$. The continuity equation implies that

$$Q(\bar{k},\bar{k}') = -Q(\bar{k}',\bar{k})\,.$$

2. 2 Symmetries

At times we shall refer to the three spatial locations as $\bar{x}_1$, $\bar{x}'$, $\bar{x}''$. At other times, using the homogeneity, we shall refer to the first point as (0, 0, 0), the second point as $\bar{x}$ and the third point as $\bar{x}'$. There are a number of symmetries which hold under the assumption of isotropy for third-order moments or third-order spectra. We shall first derive these for third-order moments. In Fig. 1 the coordinate axes are indicated as well as velocities at three spatial locations. At location $\bar{x}$ the velocity is given in the x_1 and x_2 directions. At locations $\bar{x}'$ and $\bar{x}''$ only velocity in the x_1 direction is given. The velocities indicated in Fig. 1 correspond to the experimentally measured velocity components. First notice that the three-point correlation:

$$C_{111}(\bar{x}, \bar{x}', \bar{x}'') = E\{v_1(\bar{x})\, v_1(\bar{x}')\, v_1(\bar{x}'')\}$$

$$= C_{111}(x_1'-x_1,\ x_1''-x_1;\ x_2'-x_2,\ x_2''-x_2;\ x_3'-x_3,\ x_3''-x_3\}$$

by stationarity in the spatial variables (homogeneity). Isotropy implies that we can change the coordinate system (x_1, x_2, x_3) by permuting any of the coordinate axes. Interchanging the x_1 and x_2 axes we obtain

$$E\{v_2(x_2, x_1, x_3)\, v_2(x_2', x_1', x_3')\, v_2(x_2'', x_1'', x_3'')\}$$

$$= C_{222}(x_2'-x_2,\ x_2''-x_2;\ x_1'-x_1,\ x_1''-x_1;\ x_3'-x_3,\ x_3''-x_3)\ .$$

Thus

$$C_{111}(x_1'-x_1,\ x_1''-x_1;\ x_2'-x_2,\ x_2''-x_2;\ x_3'-x_3,\ x_3''-x_3)$$

$$= C_{222}(x_2'-x_2,\ x_2''-x_2;\ x_1'-x_1,\ x_1''-x_1;\ x_3'-x_3,\ x_3''-x_3)$$

$$= C_{333}(x_3'-x_3,\ x_3''-x_3;\ x_2'-x_2,\ x_2''-x_2;\ x_1'-x_1,\ x_1''-x_1)$$

by interchanging x_1 and x_3 axes. Also

$$C_{211}(\bar{x}, \bar{x}', \bar{x}'')$$

$$= E\{v_2(x_1, x_2, x_3)\, v_1(x_1', x_2', x_3')\, v_1(x_1'', x_2'', x_3'')\}$$

$$= C_{211}(x_1'-x_1,\ x_1''-x_1;\ x_2'-x_2,\ x_2''-x_2;\ x_3'-x_3,\ x_3''-x_3)$$

$$= C_{122}(x_2'-x_2,\ x_2''-x_2;\ x_1'-x_1,\ x_1''-x_1;\ x_3'-x_3,\ x_3''-x_3)$$

(by interchanging x_1 and x_2 axes)

$$= C_{311}(x_1'-x_1,\ x_1''-x_1;\ x_3'-x_3,\ x_3''-x_3;\ x_2'-x_2,\ x_2''-x_2)$$

(by interchanging x_2 and x_3 axes)

$$= C_{233}(x_3'-x_3,\ x_3''-x_3;\ x_2'-x_2,\ x_2''-x_2;\ x_1'-x_1,\ x_1''-x_1)$$

(by interchanging x_1 and x_3 axes)

$$= C_{133}(x_2'-x_2,\ x_2''-x_2;\ x_3'-x_3,\ x_3''-x_3;\ x_1'-x_1,\ x_1''-x_1)$$

(by the permutation (x_1, x_2, x_3) to (x_3, x_1, x_2))

$$= C_{322}(x_3'-x_3,\ x_3''-x_3;\ x_1'-x_1,\ x_1''-x_1;\ x_2'-x_2,\ x_2''-x_2)$$

(by the permutation (x_1, x_2, x_3) to (x_2, x_3, x_1)) .

Now, let

$$B_{\alpha\beta\beta}(\bar{k}, \bar{k}')\, d\bar{k}\, d\bar{k}' = E\,\{ dz_\alpha(\bar{k}-\bar{k}')\, dz_\beta(-\bar{k})\, dz_\beta(\bar{k}') \} \quad .$$

A simple heuristic argument implies

$$dz_\alpha(\bar{k}) \cong \frac{1}{(2\pi)^3} \int e^{-i\bar{k}\cdot\bar{x}}\, v_\alpha(\bar{x})\, d\bar{x}$$

so that

$$B_{\alpha\beta\beta}(\bar{k}, \bar{k}') = E \int e^{-i(\bar{k}-\bar{k}')\cdot\bar{x}}\, v_\alpha(\bar{x})\, d\bar{x} \cdot \int e^{i\bar{k}\cdot\bar{x}'}\, v_\beta(\bar{x}')\, d\bar{x}' \cdot \int e^{-i\bar{k}'\cdot\bar{x}''}\, v_\beta(\bar{x}'')\, d\bar{x}''$$

$$= \frac{1}{(2\pi)^6} \int e^{i\bar{k}\cdot\bar{r} - i\bar{k}'\cdot\bar{r}'}\, C_{\alpha\beta\beta}(\bar{r}, \bar{r}')\, d\bar{r}\, d\bar{r}'$$

where $\bar{r} = \bar{x}' - \bar{x}$, $\bar{r}' = \bar{x}'' - \bar{x}$.

The symmetry relations among $C_{\alpha\beta\beta}$ imply

$$
\begin{aligned}
B_{111}(\bar{k}, \bar{k}') &= B_{111}(k_1, k_1'; k_2, k_2'; k_3, k_3') \\
&= B_{222}(k_2, k_2'; k_1, k_1'; k_3, k_3') \\
&= B_{333}(k_3, k_3'; k_2, k_2'; k_1, k_1')
\end{aligned}
$$

and

$$
\begin{aligned}
B_{211}(k_1, k_1'; k_2, k_2'; k_3, k_3') &= B_{122}(k_2, k_2'; k_1, k_1'; k_3, k_3') \\
&= B_{311}(k_1, k_1'; k_3, k_3'; k_2, k_2') \\
&= B_{133}(k_2, k_2'; k_3, k_3'; k_1, k_1') \\
&= B_{233}(k_3, k_3'; k_2, k_2'; k_1, k_1') \\
&= B_{322}(k_3, k_3'; k_1, k_1'; k_2, k_2')
\end{aligned}
$$

3. Monte Carlo and Computational Methods

Velocities $v_1(0,0,0;t)$, $v_2(0,0,0;t)$, $v_1(0,x_2,x_3;t)$ and $v_1(0,x_2',x_3';t)$ were measured as functions of time t at the fixed locations $(0,0,0)$, $(0,x_2,x_3)$, and $(0,x_2',x_3')$. The x_1 and x_2 axes represent downstream and perpendicular directions, respectively. The velocities as functions of time t can be interpreted as functions of spatial coordinate x_1 by using Taylor's hypothesis $x_1 = Ut$, where U is the mean downstream velocity. This is essentially a "frozen-flow" approximation where the velocity is measured at a fixed location, and the turbulent velocity field is swept past at a uniform speed U. The frequency spectrum of the fluctuating velocity can be interpreted as the wave-number spectrum of the fluctuating velocity component in the downstream direction (Batchelor, 1953). The choice of (x_2,x_3) and (x_2',x_3') is determined by a Monte Carlo method such that each coordinate x_2, x_3, x_2', x_3' is uniformly distributed on ±1.0 inches. There are 100 such pairs $((x_2,x_3),(x_2',x_3'))$. Later, this was augmented with seven more pairs with each coordinate uniformly distributed within ±0.333 inches. The seven pairs were added to enhance the resolution at small spatial separations.

Let

$$b_{\alpha\beta\beta}(k_1,k_1';x_2,x_3;x_2',x_3')$$

$$= \frac{1}{(2\pi)^2} \iint e^{i(k_1x_1 - k_1'x_1')} E\{v_\alpha(0,0,0)\, v_\beta(x_1,x_2,x_3)\, v_\beta(x_1',x_2',x_3')\}\, dx_1\, dx_1'$$

and

$$F_{\alpha}(k,\bar{x}) = \sum_{t=0}^{N-1} v_{\alpha}(x_1, x_2, x_3; t) \exp\{-itk\, 2\pi/N\}$$

$$\tilde{F}_{\alpha}(k_1; x_2, x_3) = F_{\alpha}(Uk_1; x_2, x_3)$$

where U is the mean downstream velocity. Then

$$b_{\alpha\beta\beta}(k_1, k'; x_2, x_3; x_2', x_3')$$

$$\cong \tilde{F}_{\alpha}(k_1 - k_1'; 0, 0)\, \tilde{F}_{\beta}(-k_1; x_2, x_3)\, \tilde{F}_{\beta}(k_1'; x_2', x_3')$$

Suppose we have N pairs $(x_2^{(j)}, x_3^{(j)})$, $(x_2'^{(j)}, x_3'^{(j)})$, $j = 1, \ldots, N$ obtained by Monte Carlo. Then

$$B_{\alpha\beta\beta}(\bar{k}, \bar{k}') = E\{dz_{\alpha}(\bar{k}, -\bar{k}')\, dz_{\beta}(-\bar{k})\, dz_{\beta}(\bar{k}')\}$$

$$= \frac{1}{(2\pi)^6} \int e^{i\bar{k}\cdot\bar{r} - i\bar{k}'\bar{r}'} C_{\alpha\beta\beta}(\bar{r}, \bar{r}')\, d\bar{r}\, d\bar{r}'$$

$$= \frac{1}{(2\pi)^6} \iiiint \exp\{i(k_2 r_2 + k_3 r_3 - k_2' r_2' - k_3' r_3')\}$$

$$\cdot \left[\iint \exp\{i(k_1 r_1 - k_1' r_1')\}\, C_{\alpha\beta\beta}(r_1, r_1'; r_2, r_2'; r_3, r_3')\, dr_1\, dr_1'\right]$$

$$\cdot\, dr_2\, dr_3\, dr_2'\, dr_3'$$

$$= \frac{1}{(2\pi)^4} \iiiint \exp\{i(k_2 r_2 + k_3 r_3 - k_2' r_2' - k_3' r_3')\}$$

$$\cdot\, b_{\alpha\beta\beta}(k_1, k_1'; r_2, r_3; r_2', r_3')\, dr_2\, dr_3\, dr_2'\, dr_3'$$

We estimate $B_{\alpha\beta\beta}(\bar{k}, \bar{k}')$ by

$$B_{\alpha\beta\beta}(\bar{k}, \bar{k}') \cong \left(\frac{2}{3}\right)^4 \frac{1}{N(I)} \sum_{j \in I} b_{\alpha\beta\beta}(k_1, k_1'; x_2^{(j)}, x_3^{(j)}; x_2^{(j)}, x_3^{(j)})$$

$$\cdot \exp\{i(k_2 x_2^{(j)} + k_3 x_3^{(j)} - k_2' x_2'^{(j)} - k_3' x_3'^{(j)})\}$$

$$+ \frac{16 - (2/3)^4}{N(E)} \sum_{j \in E} b_{\alpha\beta\beta}(k_1, k_1'; x_2^{(j)}, x_3^{(j)}; x_2'^{(j)}, x_3'^{(j)})$$

$$\cdot \exp\{i(k_2 x_2^{(j)} + k_3 x_3^{(j)} - k_2' x_2'^{(j)} - k_3' x_3'^{(j)})\}$$

for $\alpha = 1, 2$ and $\beta = 1$ where $N(I) = 11$ = number of pairs $(x_2^{(j)}, x_3^{(j)}; x_2'^{(j)}, x_3'^{(j)})$ which lie in I

$$I = \left[-\frac{1}{3}, \frac{1}{3}\right]^4 \quad ,$$

$$E = [-1, 1]^4 - I, \quad N(E) = 96 \ .$$

Because additional points were taken in I, different weights are applied here. The details of the Monte Carlo locations are given in Sec. 5.

If $\bar{k} = (k_1, k_2, k_3)$, $\bar{k}' = (k_1', k_2', k_3')$, then by the methods described above, estimates are obtained of

$$B_{111}(\bar{k}, \bar{k}') = B_{111}(k_1, k_1'; k_2, k_2'; k_3, k_3')$$

and

$$B_{211}(\bar{k}, \bar{k}') = B_{211}(k_1, k_1'; k_2, k_2'; k_3, k_3')$$

By the discussion in Sec. 2 it follows that

$$B_{221}(\bar{k},\bar{k}') = B_{111}(k_2,k_2';\, k_1,k_1';\, k_3,k_3')$$

$$B_{333}(\bar{k},\bar{k}') = B_{111}(k_3,k_3';\, k_2,k_2';\, k_1,k_1')$$

$$B_{122}(\bar{k},\bar{k}') = B_{211}(k_2,k_2';\, k_1,k_1';\, k_3,k_3')$$

$$B_{311}(\bar{k},\bar{k}') = B_{211}(k_1,k_1';\, k_3,k_3';\, k_2,k_2')$$

$$B_{133}(\bar{k},\bar{k}') = B_{211}(k_2,k_2';\, k_3,k_3';\, k_1,k_1')$$

$$B_{233}(\bar{k},\bar{k}') = B_{211}(k_3,k_3';\, k_2,k_2';\, k_1,k_1')$$

$$B_{322}(\bar{k},\bar{k}') = B_{211}(k_3,k_3';\, k_1,k_1';\, k_2,k_2')$$

Now

$$Q(\bar{k},\bar{k}') = \sum_{\alpha,\beta} Q_{\alpha\beta}(\bar{k},\bar{k}')$$

can be determined from

$$Q_{\alpha\beta}(\bar{k},\bar{k}') = k_\alpha \operatorname{Im} B_{\alpha\beta\beta}(\bar{k},\bar{k}') \quad .$$

Estimates of bias and variance of $B_{\alpha\beta\beta}(\bar{k},\bar{k}')$ are given in the appendix.

To simplify the final presentation and further reduce the variance a Monte Carlo shell integration was carried out. We compute

$$
\begin{aligned}
P(r, r') &= P(|\bar{k}|, |\bar{k}'|) \\
&= \int_{|\bar{k}| = r} \int_{|\bar{k}'| = r'} Q(\bar{k}, \bar{k}') \, d\bar{k} \, d\bar{k}' \\
&\cong \frac{1}{n} \sum_{j=1}^{n} Q(\bar{k}^j, \bar{k}'^j)
\end{aligned}
$$

with $\bar{k}^j, \bar{k}'^j$ independent and uniformly distributed on spheres with radii r and r', respectively.

The net rate of spectral energy transfer at $|\bar{k}| = r$ is

$$
\begin{aligned}
P(|\bar{k}|) = P(r) &= \int P(r, r') \, dr' \\
&\simeq \sum_{i=1}^{m} P(r, r_i') \quad .
\end{aligned}
$$

where the r_i' are given by an auxilliary Monte Carlo procedure. This is to simulate the uniform integration on the sphere.

4. Numerical Implementation

The single wire sensor locations $(0, x_2, x_3)$ and $(0, x_2', x_3')$ were determined by a Monte Carlo technique. The IMSL subroutine GGUW for generating uniformly distributed random numbers was used to generate 4×100 points in the square ±1 in. by ±1 in. and 4×7 points in a square ± 1/3 in. by ±1/3 in. Velocities were measured at locations $((0,0,0), (0, x_2^j, x_3^j), (0, x_2'^j, x_3'^j))$ for $j = 1, \ldots, 107$ and are shown in Fig. 2. Eleven of them have all coordinates of length less than 1/3 inch. An x-wire located at (0, 0, 0) was used to measure both downstream and perpendicular velocities v_1^j, v_2^j and single wires located $(0, x_2^j, x_3^j)$ and $(0, x_2'^j, x_3'^j)$ only downstream velocities v_1^j, $v_1'^j$ were measured. Compute

$$b^j_{\alpha 11}(k_1, k_1'; x_2^j, x_3^j; x_2'^j, x_3'^j) = b^j_{\alpha 11}(k_1, k_1')$$

$$= F_\alpha(k_1 - k_1'; 0; 0)\, F_1(-k_1; x_2^j, x_3^j)\, F_1(k_1'; x_2'^j, x_3'^j), \quad \alpha = 1, 2$$

where

$$F_\alpha(k; x_2, x_3) = \sum_{t=0}^{N-1} v_\alpha(0, x_2, x_3; t) \exp\{-itk\, 2\pi/N\}$$

with $N = 4096$ for

$$k_1 = 26, 76, \ldots, 976$$

$$k_1' = -976, \ldots, -26, 26, 76, \ldots, 976 \quad .$$

We obtained

$$\bar{b}^{j}_{\alpha 11}(k_1, k_1') = \frac{1}{50 \times 50} \sum_{m=k_1-25}^{k_1+25} \; \sum_{n=k_1'-25}^{k_1'+25} b^{j}_{\alpha 11}(m, n)$$

for $\alpha = 1, 2,\ j = 1, \ldots, 107$ as our basic computational data base.

$\mathrm{Im}\, \tilde{B}_{111}(\bar{k}, \bar{k}')$

$$= \sum_{j=1}^{107} \omega_j \, \mathrm{Im}\, \bar{b}^{j}_{111}(k_1, k_1') \cdot \cos\{k_2 x_2^j + k_3 x_3^j - k_2' x_2'^j - k_3' x_3'^j\}$$

is computed where

$$\omega_j = \begin{cases} \left(\frac{2}{3}\right)^4 \frac{1}{N(I)} & \text{if } j \in I \\ \left(16 - \left(\frac{2}{3}\right)^4\right) \frac{1}{N(E)} & \text{if } j \in E \end{cases} .$$

In this computation only the imaginary part of $\bar{b}^{j}_{111}(k_1, k_1')$ is considered. The real part of $\bar{b}^{j}_{111}$ is zero by the isotropic assumption and this is confirmed by the statistical resolution of the data. Similarly,

$\mathrm{Im}\, \tilde{B}_{211}(\bar{k}, \bar{k}')$

$$= \sum_{j=1}^{107} \omega_j \, \mathrm{Re}\, \bar{b}^{j}_{211}(k_1, k_1') \cdot \sin\{k_2 x_2^j + k_3 x_3^j - k_2' x_2'^j - k_3' k_3'^j\}$$

since $\mathrm{Im}\, \bar{b}^{j}_{211} = 0$ under the isotropic assumption. All other $\mathrm{Im}\, \tilde{B}_{\alpha\beta}(\bar{k}, \bar{k}')$ computations are carried out in a similar fashion using the symmetry conditions indicated in Sec. 3 giving

$$\tilde{Q}(\bar{k}, \bar{k}') = \sum_{\alpha,\beta} \tilde{Q}_{\alpha\beta}(\bar{k}, \bar{k}')$$

with

$$\tilde{Q}_{\alpha\beta}(\bar{k}, \bar{k}') = k_\alpha \operatorname{Im} \tilde{B}_{\alpha\beta\beta}(\bar{k}, \bar{k}') \quad .$$

To do the spherical shell integration, we use the GGSPH subroutine in the International Mathematical and Statistical Library to generate uniform points $\bar{k}^j, \bar{k}'^j$, $j = 1, \ldots, 2000$ on spheres with radii r and r'.

Finally,

$$\tilde{Q}(r, r') = \tilde{Q}(|\bar{k}|, |\bar{k}'|)$$

$$= \frac{1}{10} \sum_{m=1}^{10} \tilde{Q}_m(r, r')$$

where

$$\tilde{Q}_m(r, r') = \frac{1}{200} \sum_{j=100(m-1)+1}^{100m} \tilde{Q}(\bar{k}^j, \bar{k}'^j)$$

represents estimated net energy transfer from the spherical shell with radius r' to spherical shell r. This format was chosen so as to permit estimating the variance of $\tilde{Q}(r, r')$.

5. Experimental Methods

The experimental conditions were chosen to match the conditions used previously at the University of California at San Diego by Helland et al. (1979). These conditions are nearly identical to a number of studies carried out by the authors and also by a number of other investigators. The experiment was performed in the 76 cm by 76 cm by 9 m test section of the low-turbulence wind tunnel in the Department of Applied Mechanics and Engineering Sciences. A biplane grid of round, polished dural rods was located 2.4 m from the end of the contraction section. The grid had a mesh size M of 5.08 cm with rods 0.953 cm diameter. A DISA model 55P1 x-wire sensor measuring two components of velocity (v_1 and v_2) was oriented with the plane of the x parallel to the wind tunnel walls and was located at a downstream distance X/M = 48, where X is the longitudinal distance from the plane of the grid. Two single hot-wire sensors DISA model 55P01 were mounted so that each sensor could be moved with two degrees of freedom to any point in the transverse plane intersecting the x-wire sensor.

The x-wire sensor was held fixed on the tunnel centerline by a symmetrical airfoil extending horizontally through a slot in the side wall of the tunnel. The x-wire sensor was attached to a shaft passing through the center of the airfoil. The shaft permitted rotating the x-wire in the vertical plane thereby providing a method for calibrating the x-wire sensor over a range of yaw angles. A large protractor mounted outside the tunnel was used to read the yaw angle to about ± 0.1 degree of arc. One of the single wire sensors was mounted on a second airfoil support mounted outside the tunnel. A vertical slot in the wind tunnel wall permitted vertical motion of the airfoil, while the horizontal positioning was obtained by moving the airfoil back and forth through the tunnel wall on a set of bearings. The vertical slot was sealed by a sliding plate system which prevented air flow out of the wind tunnel. The other single wire sensor was mounted on a standard machinist's height gauge which was modified to hold the hot-wire support and moved in the vertical transverse direction. The height gauge was mounted on a Unislide base which moved in the horizontal transverse direction.

The position of each single wire sensor was measured relative to the location of the x-wire sensor location $\vec{x} = (0, 0, 0)$ by four dial indicators which could be read to ±0.0001 inches. The dial indicators were adjusted to be direct reading in the following manner: First the two single wires were moved so they were in the same longitudinal plane perpendicular to the wind tunnel floor passing through the plane of the x-wire sensor. This was accomplished by observing the four wires through a Gaertner traveling microscope. The two horizontal dial indicators were then set to read zero. Next the vertical positions of the two single wire sensors were measured with the traveling microscope, and the two vertical dial indicators were set to read the measured values. The single wire locations were measured before and after each series of experiments. The repeatability was good to about ±0.001 inch. Tighter tolerances in positioning the hot-wires would require a more rigid support system.

A pitot tube pressure sensor operated by a MKS Baratron electronic manometer was used to read the mean speed U. The 5 μm diameter by 1.25 mm sensing length hot-wires were operated by four DISA 55M01 constant-temperature anemometers, and the anemometer outputs were linearized by four DISA 55D10 linearizers. A Honeywell 7600 FM analog tape recorder was operated at 3-3/4 in./sec for the hot-wire calibrations and at 15 in./sec for the turbulence data giving an effective bandwith of 5 kHz.

Calibrations were performed on the hot wire sensors before and after each experiment with the grid removed from the wind tunnel. During preliminary testing the x-wire probe was set to give symmetrical yaw response about the wind tunnel centerline. Each hot-wire was linearized and the sensitivities were adjusted to be nearly identical. This enhanced the usual sum and difference decomposition approximation for x-wire calibration, but this was not an essential step because the analog sum and difference signals were not used to separate the anemometer voltage signals into the longitudinal (v_1) and vertical (v_2) velocity components. Instead the x-wire sensor was calibrated by setting the mean wind speed using the pitot-Baratron instrument to one of $\{6.0, 6.5, 7.0, 7.5, 8.0, 8.5, 9.0\}$ m/sec and then rotating the x-wire sensor through angles $\{0, \pm 1, \pm 3, \pm 5, \pm 7\}$ degrees. The wind tunnel speed was then changed, and the x-wire sensor repeatedly yawed through the set of angles. Approximately 63 pairs of mean speeds and yaw angles were used to define the full two-dimensional calibration of the x-wire. This calibration technique minimized the assumptions needed to interpret the output of x-wire sensors and we were not required to assume that the sensors were identical or mounted exactly at 90 degrees to each other. The calibration data were analyzed by standard linear regression techniques to obtain the constants (a, b, c's) for the calibration equations to first-order in anemometer voltage

$$v_1(0, 0, 0; t) = a + b\, e_1(t) + c\, e_2(t)$$

$$v_2(0, 0, 0; t) = a' + b' e_1(t) - c' e_2(t)$$

$$v_1(0, x_2, x_3; t) = a'' + b'' e_3(t)$$

$$v_1(0, x_2', x_3'; t) = a''' + b''' e_4(t)$$

where e_i is the linearized hot-wire voltage of hot-wire channel i. Channels 1 and 2 correspond to the two x-wire voltages, and channels 3 and 4 corresponded to the two single wire voltages. The assumption of first-order dependence in the calibration equations was tested by performing a regression which included the second-order terms involving e_i and comparing the results to the first-order analysis. An additional check was made by comparing some of the bispectra calculated from an identical portion of the data from a first-order calibration to one done using the second-order calibrations. The differences were found to be negligible in both cases.

The sets of uniformly distributed points shown in Fig. 2 were grouped in such a manner that the experiments could be performed efficiently. For example, the coordinates were grouped so that the sensor locations falling in the first quadrant were referred to as Case 1, and sensor locations falling in the first and second quadrants were referred to as Case 2, and so on. Each pair of coordinates was assigned a number within each case such as Case 1.1, 1.2, etc. A check was performed on the computer generated coordinates which assured us that the distribution of points was uniform within the standard deviation expected for the sample size.

The turbulence data for the 107 pairs of single sensor locations were measured in a series of seven experiments. The data were taken at night between 6 PM and 7 AM to ensure that the wind tunnel temperature variation did not exceed ±0.1°C. Data were recorded on analog tape for a ten minute interval at each pair of sensor locations. The entire series of experiments was set up and performed during a 6 week period during the Fall of 1978.

The hot-wire calibrations for all seven experiments were digitized onto a single digital tape using an Interdata 7/16 minicomputer based data acquisition system having 12-bit resolution. The turbulence data were digitized at a sample rate of 4098 samples/sec, 4096 samples/channel/record and 250 records per sensor location. Analog low-pass filtering at a cut-off frequency of 2 kHz was used during the digital recording process to minimize aliasing. A standard format was adopted putting two sensor locations on each digital tape giving a total of 54 digital tapes required to contain the turbulence data. The digital tapes were shipped to the

Lawrence Berkeley Laboratory CDC 7600 computer located in Berkeley, California, and processed remotely from San Diego using both remote dial-up access and a remote batch terminal located in the NORPAX building at the University of California, San Diego. Most of the computer output, including graphical computer output, was written to standard 48X power microfiche. The microfiche made it possible to process and store the several thousand pages of printed and graphical computer output.

6. Discussion

One-dimensional Spectra

Power spectra, probability densities, and third- and fourth-order moments were computed for the 107 pairs of hot-wire positions in order to check the quality of the data. Several positions have been selected and sample results will be shown only for those locations. Table 1 specifies the selected locations, and Table 2 shows some typical moments and characteristic length scales for the flow conditions The power spectra are shown in Fig. 3 for the three locations. The power spectra for channels 1, 3, 4, measuring the velocity in the x direction, are almost indistinguishable from each other as expected. This is a result of the homogeneity of the flow field in the transverse direction. There is no variation in the spectral shapes among the three locations which represent very close, intermediate, and distant probe locations. This result suggests that no probe interference is apparent in the second-order spectral data. Channel 2 is the spectrum of the velocity fluctuation in the x_2 direction and should not correspond to the spectra in the x_1 direction even under the assumption of full isotropy. Again there is no evidence for probe interference problems in the x_2-component spectra. Note that graphs and tables are expressed in frequency while the initial derivations of the paper are in terms wavenumber.

The probability density functions are shown for the selected three locations in Fig. 4. The density functions have each been normalized by the standard deviation for each channel. All density functions plotted in this manner for each location are coincident and nearly Gaussian in shape.

Note that again there is no apparent variation in the density curves across the three probe locations. While the deviation from Gaussianity appears slight, it is important that there be some deviation so that energy transfer among fluctuations of various scales may exist consistent with a three-dimensional turbulent field.

An elaborate check on second-order isotropy was made using about 20% of the hot-wire locations covering the range from $|\vec{r}|$ small to $|\vec{r}|$ large. From Batchelor (1953) it is easily shown that the cross-spectra between the x-wire sensor and a sensor placed at $\vec{r} = (0, r_2, r_3)$ can be computed from an estimate of the downstream and transverse correlations f and g

$$u^2 f(r) = E\, v_1(\vec{x})\, v_1(\vec{x} + \vec{r})$$

$$u^2 g(r) = E\, v_2(\vec{x})\, v_2(\vec{x} + \vec{r})$$

where f and g are functions of $r = |\vec{r}|$, the separation between the two sensors and $u^2 = \mathrm{var}(\vec{v})$. Then by isotropy we can write

$$R_{ij}(\vec{r}) = u^2\left(\frac{f - g}{r^2} \cdot r_i r_j + g\, \delta_{ij}\right)$$

and

$$g = f + \frac{1}{2} r f' , \quad f' = \frac{\partial f}{\partial r} .$$

Thus the cross spectrum between downstream velocity components $v_1(0, 0, 0)$ and $v_1(0, x_2, x_3)$ can be expressed in terms of f and g

$$\phi_{1,1}(k_1, r_2, r_3) = \frac{u^2}{2\pi}\int_{-\infty}^{\infty} -\frac{1}{2}\frac{f'}{r} r_1^2 e^{ik_1 r_1} dr + \frac{u^2}{2\pi}\int_{-\infty}^{\infty} g\, e^{ik_1 r_1} dr_1 .$$

Similarly the cross spectrum between velocity components $v_2(0,0,0)$ and $v_1(0, x_2, x_3)$ is given by

$$\phi_{2,1}(k_1, r_2, r_3) = \frac{u^2}{2\pi}\int_{-\infty}^{\infty} \frac{f - g}{r^2}\, r_1 r_2\, e^{ik_1 r_1} dr_1 .$$

The correlations f and g are shown in Fig. 5 for the Cases 4.10 in both linear and semilogarithmic coordinates. The agreement among the correlations is excellent with Case 4.10, and 4.10 was used to perform the isotropy checks which follow.

The directly estimated cross spectra are compared with the cross spectra computed using the assumption of isotropy are shown in a series of figures for the three cases of small, intermediate, and wide separation. The results are shown on linear scales in Figs. 6 to 8 to show the comparison at low frequency. The results are repeated on semi-logarithmic scales in Figs. 9 to 11 where the cross spectra have been multiplied by the frequency to show the comparison at high frequency. The agreement is generally good, with some significant deviations occurring at the higher frequencies. While the assumption of isotropy (and Taylor's hypothesis) for these computations appears reasonably well satisfied, it is impossible to know the significance of deviations on the integrity of the third-order energy transfer computations where the assumption of full isotropy is required.

The bispectra b_{111} and b_{211} for the three locations are shown in Figs. 12 to 14. The bispectra do vary with probe locations now since they involve three velocities, one from each point (0, 0, 0), $(0, x_2, x_3)$, and $(0, x_2', x_3')$. The magnitude of each bispectral type does not change much with position (all bispectra figures have the same scales), but the "width" of the peak does change rapidly with increasing probe separation. The larger the separation the smaller the extent of the main lobe of the bispectral peaks. The variation with probe separation is more readily observed in diagrams of the statistical resolution of the bispectra b_{111} and b_{211} shown in Tables 3 to 5. In the resolution diagrams, the numbers represent the rounded ratio of the bispectral estimate to the standard deviation of the estimate. The sign is the sign of the bispectrum.

The results of the computations for $Q(k, k')$ are shown in Tables 6 and 7 and in Figs. 15-19. Table 6 shows the magnitude Q and the standard deviation of Q is shown in parentheses. The truncated ratio of the magnitude of Q with its standard deviation is shown in Table 7. Figures 15-19 show representative cross-section plots of the data in Table 6. The curves represent energy transfer from a frequency magnitude, f', to a selected frequency f. For $f' < f$ we expect most of the energy transfer to be positive, that is a loss of energy from the low frequencies to the higher frequencies; for $f' > f$ we expect most of the energy transfer to be negative, that is, a gain of energy in the higher frequencies from the lower frequencies. The continuity equation requires that $Q = 0$ when $f = f'$. This requirement is approximately satisfied in Figs. 17 and 18. In Figs. 15, 16, and 19 the Q differs significantly from zero when $f = f'$. This may be due to too broad a smoothing in the spectral estimation. In Figs. 17 and 18, the two curves are consistent with the expected direction for the energy transfer. These data are in qualitative agreement with some calculations of Deissler (1977) who used an expansion technique to estimate the shape of the net energy transfer between wavenumber shells. These computations are in the central spectral range where one would expect to have greater reliability because isotropy would probably be satisfied in this range (as contrasted with low wavenumber) and we have resolvability (as contrasted with high wavenumber).

The physical significance of this investigation is associated with the notion of energy transfer among the eddies or scales in the Fourier transform domain. Such a transfer of energy in homogeneous turbulence is an aspect of the nonlinearity in turbulence. There has been a concept of local transfer of energy employed in a number of discussions of turbulence. Though the notion has usually not been formalized, it appears to be a claim that appreciable transfer takes place only to neighboring wave numbers. Since there are three wave number vectors (with sum equal to zero) involved in the equation for dissipation and transfer of energy, this means that two of the wave number vectors are close to each other and the third is close to zero. The usual assumption has been that the transfer of energy is one-sided, from lower wave numbers to higher wave numbers (in terms of wave number vector magnitude). This does not seem to be literally confirmed by the results one has that appear to have resolution and that seem to be consistent with the usual symmetry $Q(|k|, |k'|) = -Q(|k'|, |k|)$, results obtained in an intermediate wave number range. It is true that one appears to have low variance in the low wave number range but there are fears of nontrivial bias here. In the high wave number range one has to be resigned to high relative variance. From the results it seems as if there is nontrivial interaction between wave number magnitudes differing by a factor of three.

There are a variety of questions that arise if one were to consider carrying out an experiment like this again. It would seem to be more appropriate to use two x-wires and one single wire rather than one x-wire and two single wires in the experiment. This would make the experiment a bit more difficult. However, this would allow one to estimate a 2, 2, 1 bispectrum as well as the 1, 1, 2 bispectrum. These two bispectra are related theoretically under the assumption of isotropy. However, our estimates of the 1, 1, 2 bispectrum generally had little resolution while it is clear in terms of previous experimental results that we would have good resolution for the 2, 2, 1 bispectral estimate (Helland et al. (1979)), at least for separations close to zero. We could have one fixed x-wire and let the x-wire and single wire probe float in the fixed perpendicular plane.

If one could get adequate analytic representations of the 1, 1, 1 and 2, 2, 1 bispectra as they depend on spatial separation, suggested by the estimates, the Q function would be obtained by a direct Fourier transform.

The Taylor hypothesis has been used to translate time separation into the spatial x_1 separation. Tests of the Taylor hypothesis with separation in the x_1 direction have been carried out (Favre et al. (1955), Stegen and Van Atta (1970)). In our application we do have separation in the perpendicular direction.

Should the Monte Carlo locations be laid out uniformly over a fixed range or set out in a stratified manner? If we have some knowledge about the general shape of the function to be integrated, we can use the importance sampling scheme to choose a convenient probability distribution which approximates a normalized positive integrand. If we lay out the Monte Carlo locations according to such a distribution we can get a substantial variance reduction (Kleijnen (1974), Niederreiter (1978)). Also we could take advantage of the assumed isotropy and concentrate all locations in a subregion using antithetic variates to reduce variance (Kleijnen (1974)). Quasi-random points could be used instead of the pseudo-random numbers to improve the overall convergent rate in the Fourier transform if the total variation of the integrand is not too large (Niederreiter (1978)).

One of the basic questions is that of better resolution. There is no difficulty in appreciably larger number of records (a factor of 10). A real difficulty is that of the increased computational cost. With the use of modern ultrahigh speed array processes and signal display devices operated by modest laboratory computers, the computing cost can be fixed and the computing speed is reasonable.

Appendix: Bias and Variance

In this section the bias and the variance using a Monte Carlo layout of the experiment is compared with a deterministic layout. Let

$$A_{\alpha\beta\beta}(\overline{K},\overline{K}') = \int e^{i(k_2x_2+k_3x_3-k_2'x_2'-k_3'x_3')}$$

$$\cdot\ b_{\alpha\beta\beta}(k_1,k_1';\ x_2,x_3;\ x_2',x_3')\,dx_2\,dx_3\,dx_2'\,dx_3'$$

where $\overline{K} = (k_1,k_2,k_3)\,,\quad \overline{K}' = (k_1',k_2',k_3')$

$$b_{\alpha\beta\beta}(k_1,k_1';\ x_2,x_3;\ x_2',x_3')$$

$$= \frac{1}{(2\pi)^2}\int e^{i(k_1u_1-k_1'u_1')}\ E\{v_\alpha(0,0,0)\,v_\beta(u_1,x_2,x_3)\,v_\beta(u_1',x_2',x_3')\}\,du_1\,du_1'$$

which is a one dimensional bispectrum. An estimate of $b_{\alpha\beta\beta}$ is given by

$$\hat{b}_{\alpha\beta\beta}(k_1,k_1;\ x_2,x_3;\ x_2,x_3) = \frac{(2\pi)^2}{N^2}\sum_{s_1=-\infty}^{\infty}\ \sum_{s_2=-\infty}^{\infty}\ \sum_{s_3=-\infty}^{\infty}$$

$$w_N\left(\frac{2\pi(k_1-s_1)}{N},\frac{2\pi(k_1-s_2)}{N},\frac{2\pi(k_3-s_3)}{N}\right)I^{(N)}_{\alpha\beta\beta}\left(\frac{2\pi s_1}{N},\frac{2\pi s_2}{N},\frac{2\pi s_3}{N}\right)$$

where the s_i's are such that

$$\sum_{i=1}^{3} s_i = 0$$

and

$$I^{(N)}_{a_1,a_2,a_3}(\alpha_1,\alpha_2,\alpha_3) = \frac{1}{(2\pi)^2N}\prod_{j=1}^{3} d^{(N)}_{a_j}(\alpha_j)$$

with $$d^{(N)}_{a_j}(\alpha_j) = \sum_{t=0}^{N-1} x_{a_j}(t)\, e^{-i\alpha_j t}$$

such that $\sum_{j=1}^{3} \alpha_j = 0 \pmod{2\pi}$. Here

$$w_N(u_1, u_2, u_3) = \frac{1}{h^2}\, w\left(\frac{u_1}{h}, \frac{u_2}{h}, \frac{u_3}{h}\right)$$

w is a symmetric weight function such that

$$\int w(a_1, a_2, a_3)\, \delta\left(\sum_{i=1}^{3} u_i\right) du_1 du_2 du_3 = 1 \quad .$$

It is known that (Brillinger and Rosenblatt (1967)) the bias

$$\begin{aligned}
b_N &= E\,\hat{b}_{\alpha\beta\beta}(k_1, k_1') - b_{\alpha\beta\beta}(k_1, k_1') \\
&= \frac{h^2}{2}\Bigg[\frac{\partial^2}{\partial k_1}\, b_{\alpha\beta\beta}(k_1, k_1') \cdot \int u_1^2\, w(u_1, u_2)\, du_1 du_2 \\
&\qquad + 2\,\frac{\partial^2}{\partial k_1 \partial k_1'}\, b_{\alpha\beta\beta}(k_1, k_1') \int u_1 u_2\, w(u_1, u_2)\, du_1 du_2 \\
&\qquad + \frac{\partial^2}{\partial k_1'^2}\, b_{\alpha\beta\beta}(k_1, k_1') \int u_2^2\, w(u_1, u_2)\, du_1 du_2\Bigg] \\
&\qquad + o(h^2)
\end{aligned}$$

if $b_{\alpha\beta\beta}$ is twice continuously differertiable and appropriate conditions are imposed on the weight function w. Under suitable conditions the variance

$$\operatorname{Var}(\hat{b}_{\alpha\beta\beta}(k_1, k_1')) = \frac{2\pi}{h^2 N} f_\alpha(k_1)\, f_\beta(k_1')\, f_\beta(k_1+k_1') \int w^2(u_1, u_2)\, du_1 du_2$$

$$+ O\left(\frac{1}{hN}\right)$$

where f_α is the power spectrum of component α.

To approximate $A_{\alpha\beta\beta}$, suppose a deterministic uniform grid on $[-a, a]^4$, say m^4 points, $\bar{x}_{i,j,k,\ell} = (x_i, x_j; x_k', x_\ell')$, are given. Then a natural approximation of $A_{\alpha\beta\beta}$ is given by

$$A^*_{\alpha\beta\beta}(\bar{K}, \bar{K}') = \frac{(2a)^4}{m^4} \sum_{i,j,k,\ell=1}^{m} \exp\{i(k_2x_i + k_3x_j - k_2'x_k' - k_3'x_\ell')\}$$

$$\cdot\ \hat{b}_{\alpha\beta\beta}(k_1, k_1'; x_i, x_j ; x_k', x_\ell') \quad ,$$

$$E\, A^*_{\alpha\beta\beta}(\bar{K}, \bar{K}') = \frac{(2a)^4}{m^4} \sum_{i,j,k,\ell=1}^{m} \exp\{i(k_2x_i + k_3x_j - k_2'x_k' - k_3'x_\ell')\}$$

$$\cdot\ \{b_{\alpha\beta\beta}(k_1, k_1'; x_i, x_j; x_k', x_\ell') + O(h^2)\}$$

$$= A_{\alpha\beta\beta}(\bar{K}, \bar{K}') + O(h^2) + O\left(\frac{1}{m^2}\right)$$

if one can assume $b_{\alpha\beta\beta}$ twice continuously differentiable. Now we assume the independence of measurements at different locations. This is reasonable since the measurements at different locations are taken at different times. Then

$$\mathrm{Var}(A^*_{\alpha\beta\beta}(K,K') = \left(\frac{2a}{m}\right)^8 \sum_{i,j,k,\ell=1}^{m} \mathrm{Var}(\hat{b}_{\alpha\beta\beta}(k_1,k_1',x_i,x_j;\,x_k',x_\ell'))$$

$$= \left(\frac{2a}{m}\right)^8 \sum_{i,j,k,\ell=1}^{m} \left\{ \frac{2\pi}{h^2N} f_\alpha(k_1)\, f_\beta(k_1)\, f_\beta(k_1+k_1') \int w^2(u_1,u_2)\,du_1\,du_2 + O\left(\frac{1}{hN}\right) \right\}$$

$$= \left(\frac{2a}{m}\right)^4 \left\{ \frac{2\pi}{h^2N} \; f_\alpha(k_1)\, f_\beta(k_1')\, f_\beta(k_1+k_1') \int w^2(u_1,u_2)\,du_1\,du_2 \right.$$

$$\left. + O\left(\frac{a^2}{m^2}\right) + O\left(\frac{1}{hN}\right) \right\} \; .$$

Now suppose a uniform random sample of M points from $[-a,a]^4$ are taken, say, $\bar{x}_j = (x_{2j}, x_{3j};\, x_{2j}', x_{3j}')$, $j = 1,\ldots,M$. Then a Monte Carlo approximation of $A_{\alpha\beta\beta}(\bar{K},\bar{K}')$ is given by

$$B^* = B^*_{\alpha\beta\beta}(\bar{K},\bar{K}') = \frac{(2a)^4}{M} \sum_{j=1}^{M} \exp\{i(k_2x_{2j} + k_3x_{3j} - k_2'x_{2j}' - k_3'x_{3j}')\}$$

$$\cdot\; \hat{b}_{\alpha\beta\beta}(k_1,k_1';\,\bar{x}_j)$$

$$EB^* = E_{\bar{x}_j}\,\{E(B^* \mid \bar{x}_j)\}$$

$$= E_{x_j}\left\{ \frac{(2a)^4}{M} \sum_{j=1}^{M} \exp\{i(k_2x_{2j}+k_3x_{3j} - k_2'x_{2j}' - k_3'x_{3j}')\}\, \hat{b}_{\alpha\beta\beta}(k_1,k_1';\,\bar{x}_j) + O(h^2) \right\}$$

$$= A_{\alpha\beta\beta}(\bar{K},\bar{K}') + O(h^2)$$

$$\mathrm{Var}(B^*) = E\,\{\mathrm{Var}(B^* \mid \bar{x}_j)\} + \mathrm{Var}\,\{E(B^* \mid \bar{x}_j)\}$$

Now

$$E[\mathrm{Var}(B^{*}\,|\bar{x}_j)] = \left\{ \frac{(2a)^8}{M^2} \sum_{j=1}^{M} \left[-\frac{2\pi}{h^2 N} f_{\alpha}(k_1)\, f_{\rho}(k_1')\, f_{\beta}(k_1 + k_1') \right.\right.$$

$$\left.\left. \cdot \int w^2(u_1, u_2)\, du_1 du_2 + O\left(\frac{1}{hN}\right) \right] \right\}$$

$$= \frac{(2a)^4\, 2\pi}{M\, h^2 N} \int f_{\alpha}(k_1; 0, 0)\, f_{\beta}(k_1'; x_2, x_3)\, f_{\beta}(k_1 + k_1'; x_2', x_3')\, dx_2 dx_3 dx_2' dx_3'$$

$$\cdot \int w^2(u_1, u_2)\, du_1 du_2 + O\left(\frac{1}{hN}\right) + O\left(\frac{1}{M}\right)$$

and

$$\mathrm{Var}\{E(B^{*}\,|\bar{x}_j)\} = \mathrm{Var} \left\{ \frac{(2a)^4}{M} \sum_{j=1}^{M} b_{\alpha\beta\beta}(k_1, k_1'; \bar{x}_j) \right.$$

$$\left. \cdot \exp\{ i(k_2 x_2 + k_3 x_3 - k_2' x_2' - k_3' x_3') + O(h^2) \right\}$$

$$= \frac{(2a)^4}{M} \int b^2_{\alpha\beta\beta}(k_1, k_1'; x_2, x_3; x_2', x_3)\, dx_2 dx_3 dx_2' dx_3' + O(h^2)$$

Therefore it appears that when 1/m is substantially less than h then the bias of deterministic layout is better than the bias of Monte Carlo layout, whereas the variances are comparable if the number of sample points are the same. When h is substantially less than 1/m then the bias of a Monte Carlo is better than that of a deterministic layout and the variances might be comparable. This depends on the choice of other parameters. Now the details of the variance will be computed to the first order. However, it must be kept in mind that each choice of a set of locations corresponds to a complete set of experimental measurements at these locations. Further the greater the number of locations, the greater the length and cost of computations. So even though it is easy to speak of 1/m small, this amounts to m^4 locations and the experimental and computational cost become enormous. This is the great advantage of the Monte Carlo procedure so as to keep experimental and

Now

$$\mathrm{Var}[\mathrm{Im}\, \hat{b}_{111}(k_1, k_1'; L_x^{(j)}) \cdot \cos\,(L_{k\cdot x}^{(j)})]$$

$$= E[\mathrm{Var}(\mathrm{Im}\, \hat{b}_{111}(k_1, k_1'; L_x^{(j)}) \cos\,(L_{k\cdot x}^{(j)}) \mid x_2, x_3, x_2', x_3')]$$

$$+ \mathrm{Var}[E(\mathrm{Im}\, \hat{b}_{111}(k_1, k_1'; L_x^{(j)}) \cos(L_{k\cdot x}^{(j)}) \mid x_2, x_3, x_2', x_3')]$$

$$= E\left\{ \sigma^2_{L_x^{(j)}} \cdot \cos^2(L_{k\cdot x}^{(j)}) \right\}$$

$$+ \mathrm{Var}\left\{ f_{111, L_x^{(j)}}(k_1, k_1') \cdot \cos(L_{k\cdot x}^{(j)}) \right\}$$

where

$$\sigma^2_{L_x^{(j)}} = \mathrm{Var}(\mathrm{Im}\, b_{111}(k_1, k_1'; L_x^{(j)}))\ ,$$

$$f_{111, L_x^{(j)}}(k_1, k_1') = E[\mathrm{Im}\, b_{111}(k_1, k_1'; L_x^{(j)})]$$

$$= \sigma^2(k_1, k_1') \int_{-a}^{a} \cos^2(L_{k-x}^{(j)}) \left(\frac{1}{2a}\right)^4 dx_2\, dx_3\, dx_2'\, dx_3'$$

$$+ \left(\frac{1}{2a}\right)^4 \int_{-a}^{a} f^2_{111, L_x^{(j)}}(k_1, k_1') \cdot \cos(L_{k\cdot x}^{(j)})\, dx_2 dx_3\, dx_2' dx_3'$$

$$- \left(\frac{1}{2a}\right)^8 \left\{ \int_{-a}^{a} f_{111, L_x^{(j)}}(k_1, k_1') \cos(L_{k\cdot x}^{(j)})\, dx_2 dx_3\, dx_2' dx_3' \right\}^2$$

Here $\sigma^2(k_1, k_1')$ is the variance of $\mathrm{Im}\, f_{111, L_x^{(j)}}(k_1, k_1')$ for all j's. This variance is independent of the location because the variance is proportional to the product of the power spectra. The previous expression equals

$$A + B - C$$

where A, B, C correspond to the 3 terms in the preceding equation. To evaluate A, drop the subscript j. Then

$$\int_{-a}^{a} \cos^2(k_2x_2 + k_3x_3 - k_2'x_2' - k_3'x_3')\, dx_2 dx_3 dx_2' dx_3'$$

$$= \int_{-a}^{a} \frac{1}{2}(\cos 2(k_2x_2 + k_3x_3 - k_2'x_2' - k_3'x_3') + 1)\, dx_2\, dx_3 dx_2'\, dx_3'$$

$$= \frac{1}{2}(2a)^4 + \frac{1}{2}\int_{-a}^{a} \cos(2k_2x_2 + 2k_3x_3 - 2k_2'x_2' - 2k_3'x_3')\, dx_2 dx_3 dx_2' dx_3' .$$

Now $\int_{-a}^{a} \cos(\alpha + \beta - \gamma - \delta)\, d\alpha\, d\beta\, d\gamma\, d\delta$

$$= \int_{-a}^{a} [\cos(\alpha+\beta) \cos(\gamma+\delta) + \sin(\alpha+\beta) \sin(\gamma+\delta)]\, d\alpha\, d\beta\, d\gamma\, d\delta$$

$$= \int_{-a}^{a} [(\cos\alpha \cos\beta - \sin\alpha \sin\beta)(\cos\gamma \cos\delta - \sin\gamma \sin\delta)$$

$$+ (\sin\alpha \cos\beta + \cos\alpha \sin\beta)(\sin\gamma \cos\delta + \cos\gamma \sin\delta)]\, d\alpha\, d\beta\, d\gamma\, d\delta$$

$$= \int_{-a}^{a} (\cos\alpha\, \cos\beta\, \cos\gamma\, \cos\delta)\, d\alpha\, d\beta\, d\gamma\, d\delta$$

since $\int_{-a}^{a} \sin \omega x\, dx = 0$ for $\omega \neq 0$. We obtain

$$A = \sigma^2(k_1, k_1') \left(\frac{1}{2a}\right)^4 \cdot \left[\frac{1}{2}(2a)^4 + \frac{1}{2}\int_{-a}^{a} \cos 2k_2x_2 \cos 2k_3x_3 \cos 2k_2'k_2' \cdot \cos 2k_3' x_3' \, dx_2 dx_3 dx_2' dx_3'\right]$$

$$= \sigma^2(k_1, k_1') \left(\frac{1}{2a}\right)^4 \left[\frac{(2a)^4}{2} + \frac{1}{2}\,\frac{1}{k_2k_3k_2'k_3'} \sin 2ak_2 \sin 2ak_3 \sin 2ak_2' \sin 2ak_3'\right]$$

$$= \frac{1}{2}\sigma^2(k_1, k_1') \left[1 + \frac{\sin 2ak_2}{2ak_2} \cdot \frac{\sin 2ak_3}{2ak_3} \cdot \frac{\sin 2ak_2'}{2ak_2'} \cdot \frac{\sin 2ak_3'}{2ak_3'}\right]$$

since $\int_{-a}^{a} \cos 2\omega x \, dx = \frac{1}{\omega} \sin 2a\omega$.

The values of B and C cannot be determined theoretically since we don't know theoretical values of $f_{111, L_x^{(j)}}(k_1, k_2)$ though we have estimated values. Now B and C may be estimated by using the estimates of $f_{111, L_x^{(j)}}(k_1, k_2)$. Note that B and C are independent of $L_x^{(j)}$ (theoretically).

In Summary:

$$\mathrm{Var}(\mathrm{Im}\, B_{111}(\bar{K}, \bar{K}')) = \frac{1}{N^2} \sum_{j=1}^{N} [A + B - C] = \frac{1}{N}(A + B - C)$$

where

$$A = \frac{1}{2}\sigma^2(k_1, k_1')\left[1 + \frac{\sin 2ak_2}{2ak_2}\cdot\frac{\sin 2ak_3}{2ak_3}\cdot\frac{\sin 2ak_2'}{2ak_2'}\cdot\frac{\sin 2ak_3'}{2ak_3'}\right]$$

$$B = \left(\frac{1}{2a}\right)^4 \int_{-a}^{a} f_{111}^2(k_1, k_1'; x_2, x_3, x_2', x_3') \cos^2(k_2x_2 + k_3x_3 - k_2'x_2' - k_3'x_3')\, dx_2\, dx_3\, dx_2'\, dx_3'$$

$$C = \left(\frac{1}{2a}\right)^8 \left[\int_{-a}^{a} f_{111}(k_1, k_1'; x_2, x_3, x_2', x_3') \cos(k_2x_2 + k_3x_3 - k_2'x_2' - k_3'x_3')\, dx_2\, dx_3\, dx_2'\, dx_3'\right]^2$$

with

$$\sigma^2(k_1, k_1') \equiv \text{variance of } \operatorname{Im} b_{111}(k_1, k_1'; L_x^{(j)})$$

$$f_{111}(k_1, k_1'; x_2, x_3, x_2', x_3') \equiv f_{111, L_x^{(j)}}(k_1, k_1')$$

$$\equiv E[\operatorname{Im} b_{111}(k_1, k_1'; x_2, x_3, x_2', x_3')] \quad .$$

We now consider

$$\operatorname{Var}[\operatorname{Im} B_{211}^*(\bar{K}, \bar{K}')]$$

$$= \operatorname{Var}\left[\frac{1}{N}\sum_{j=1}^{N} \operatorname{Re} b_{211}(k_1, k_1'; x_2^{(j)}, x_3^{(j)}, x_2'^{(j)}, x_3'^{(j)}) \sin(k_2x_2^{(j)} + k_3x_3^{(j)} - k_2'x_2'^{(j)} - k_3'x_3'^{(j)})\right]$$

where this time the imaginary part of b_{211} is zero again by the assumption of isotropy.

This equals

$$\frac{1}{N^2} \sum_{j=1}^{N} \mathrm{Var}[\mathrm{Re}\ b_{211}(k_1, k_1'; L_x^{(j)}) \cdot \sin(L_{k-x}^{(j)})]$$

where we use the same notation as before and ignore possible correlations among $b_{211}(k_1, k_1'; L_x^{(j)})$ for different j's. Carrying out the same kind of argument we have:

$$\mathrm{Var}(\mathrm{Im}\ B_{211}(\overline{K}, \overline{K}')) = \frac{1}{N}[A' + B' - C']$$

where

$$A' = \frac{1}{2} \sigma^2_{b_{211}}(k_1, k_1') \left[1 - \frac{\sin 2ak_2}{2ak_2} \cdot \frac{\sin 2ak_3}{2ak_3} \cdot \frac{\sin 2ak_2'}{2ak_2'} \cdot \frac{\sin 2ak_3'}{2ak_3'}\right]$$

$$B' = \left(\frac{1}{2a}\right)^4 \int_{-a}^{a} \mathrm{Re}\ f^2_{211}(k_1, k_1'; L_x^{(j)}) \sin^2(L_{k \cdot x}^{(j)})\, dx_2\, dx_3\, dx_2'\, dx_3'$$

$$C' = \left(\frac{1}{2a}\right)^8 \left[\int_{-a}^{a} \mathrm{Re}\ f_{211}(k_1, k_1'; L_x^{(j)}) \sin(L_{k \cdot x}^{(j)})\, dx_2\, dx_3\, dx_2'\, dx_3'\right]^2$$

with

$$\sigma^2_{b_{211}}(k_1, k_1') = \mathrm{Var}(\mathrm{Re}\ b_{211}(k_1, k_1'; L_x^{(j)}))$$

$$\mathrm{Re}\ f_{211}(k_1, k_1') = E[\mathrm{Re}\ b_{211}(k_1, k_1')]$$

Again A' can be computed from the estimated power spectra which are fairly reliable. B', C' can only be estimated empirically.

References

Batchelor, G. K. (1953) *The Theory of Homogeneous Turbulence*, Cambridge University Press.

Brillinger, D. R. and Rosenblatt, M. (1967) Computation and interpretation of k^{th} order spectra. In *Spectral Analysis of Time Series* (B. Harris, ed.), pp. 189-232, Wiley, New York.

Deissler, R. G., "On the localness of the spectral energy transfer in turbulence," NASA Technical Memorandum 73824, 1977.

Farce, A., Gariglio, J., and Dumas, R. (1955) "Some measurements of time and space correlation in wind tunnel," N. A. C. A. Tech. Memo. no. 1370.

Helland, K. N., Lii, K. S., and Rosenblatt, M. (1979) Bispectra and energy transfer in grid-generated turbulence. In *Developments in Statistics*, vol. 2 (Krishnaiah, ed.), pp. 123-155. Academic Press.

Kleijnen, Jack P. C. (1974) *Statistical Techniques in Simulation*, Part 1, Marcel-Dekker.

Lii, K. S., Rosenblatt, M., and Van Atta, C. W. (1976) Bispectral measurements in turbulence, J. Fluid Mech. 77, 45.

Niederreiter, H. (1978) "Quasi-Monte Carlo methods and pseudo-random numbers," Bull. Amer. Math. Soc. 84, 957-1041.

Stegen, G. R. and Van Atta, C. W. (1970) "Phase speed measurements in grid turbulence," J. Fluid Mech. 38, 743.

Table 1. Coordinates of four selected velocity sensor locations.

	$\bar{x}'$, inches		$\bar{x}''$, inches	
Case	x_2'	x_3'	x_2''	x_3''
6.10	-0.080	-0.100	-0.083	-0.100
5.2	+0.081	-0.926	+0.529	-0.301
8.4	-1.00	-0.980	-0.897	-0.962
4.10	+0.874	-0.818	+0.795	+0.419

Table 2. Physical parameters for grid-generated turbulent flow.

U (m/sec)	7.77	$E[u^3]/E[u^2]^{3/2}$	0.0087
V (m/sec)	0.002	$E[v^3]/E[v^2]^{3/2}$	-0.0186
M (cm)	5.08	$E[u^4]/E[u^2]^2$	2.912
d (cm)	0.953	$E[v^4]/E[v^2]^2$	2.905
R_M	25300	R_λ	34.6
x/M	48	ϵ (cm^2/sec^3)	787
$E[u^2]^{1/2}/U$	0.0163	η (cm)	0.047
$E[v^2]^{1/2}/U$	0.0142	v_k (cm/sec)	3.32
$E[u^2]^{1/2}/E[v^2]^{1/2}$	1.15	$\lambda_k = U/2\pi\eta_k$	2630

ORIGINAL PAGE IS
OF POOR QUALITY

Table 3. Resolvability of one-dimensional bispectra $b_{111}(f, f'; \bar{x}, \bar{x}', \bar{x}'')$ and $b_{211}(f, f'; \bar{x}, \bar{x}', \bar{x}'')$ for Case 6.10.

	$\mathrm{Re}\, b_{111}$																			
f′ f	25				226				326				526				726			926
-925.95	0	0	0	0	0	1	3	0	1	0	1	-1	1	0	-1	1	1	2	1	1
-825.90	2	0	1	2	1	1	2	2	-1	-1	1	0	0	1	0	-1	0	-1	-1	1
-725.85	-1	-2	0	-1	1	-2	-1	1	0	-1	-1	-1	1	-2	-3	-1	1	0	1	0
-625.81	1	0	1	1	0	-1	-1	-1	0	1	1	-2	-1	0	0	-1	-1	0	-3	-1
-525.76	2	0	1	0	-1	0	-1	1	-1	0	-1	-1	-1	-2	-1	-2	-1	0	-1	0
-425.71	2	0	1	0	-2	1	-1	0	0	-2	0	-1	-3	-1	-2	-1	-2	-1	-1	-1
-325.66	1	0	2	0	-1	-2	0	1	-1	-1	0	-1	0	-1	-1	0	-1	-2	-1	1
-225.61	1	0	0	1	0	-1	1	-1	-2	-2	0	0	-2	-2	-1	-2	-2	-1	-3	0
-125.56	1	0	-1	0	0	0	-2	1	0	0	-1	-1	-1	-1	-1	-4	-2	-2	-1	-2
-25.51	0	2	1	-2	0	0	-1	1	0	0	-1	0	-1	-2	-3	-1	0	-1	-2	0
25.51	0	0	1	1	-1	0	0	0	1	2	0	1	1	-1	0	1	-2	1	1	1
125.56	0	1	0	0	0	-1	0	0	-1	-1	1	0	0	1	-1	1	0	2	1	1
225.61	1	1	0	-1	1	0	0	0	2	2	0	-1	1	-1	1	3	2	-1	1	3
325.66	0	0	0	1	-2	0	0	1	1	1	0	-2	1	1	3	2	0	0	0	1
425.71	-1	2	0	0	-1	0	0	0	1	0	0	0	-1	-1	0	2	2	2	-1	0
525.76	1	0	0	0	0	1	0	-1	1	0	0	1	0	0	0	1	-2	-2	1	-1
625.81	1	0	0	2	-1	0	-1	-1	-1	0	-1	0	1	-1	1	1	-1	0	-2	-1
725.85	0	1	-1	0	-1	0	1	1	-1	0	0	-2	2	2	1	0	0	0	1	-1
825.90	0	1	-1	0	1	-1	-1	1	-2	0	0	1	2	-1	1	1	-1	0	-1	-1
925.95	-1	1	0	0	0	-1	-1	0	0	0	0	1	0	0	1	1	1	0	-3	0
	$\mathrm{Re}\, b_{211}$																			
-925.95	0	0	1	0	1	1	1	1	3	2	2	2	-1	3	0	0	0	1	0	1
-825.90	0	2	2	1	0	2	1	4	4	2	0	2	-1	0	0	1	3	-1	1	1
-725.85	0	-1	2	2	2	3	1	0	1	1	0	-1	-2	1	0	1	0	2	2	1
-625.81	1	2	-1	1	3	3	1	1	0	2	2	1	1	0	-1	1	-1	2	-2	-1
-525.76	1	0	1	0	1	-1	1	1	-1	1	1	1	-1	0	0	-1	-2	0	-2	-2
-425.71	1	0	0	3	2	1	0	1	0	0	-2	0	-1	-2	-1	-1	-1	-3	-2	-1
-325.66	2	1	0	1	0	2	-2	-1	0	-1	-1	0	-1	0	0	-2	-1	-2	-1	-2
-225.61	3	2	1	-1	1	0	-2	-2	-1	-3	-1	-1	-1	-2	-2	0	-1	-2	-2	-4
-125.56	2	3	-1	-1	-1	-2	-2	-1	-2	-2	-2	-2	-3	-2	-2	-2	-3	-2	-3	-1
-25.51	-1	-3	-1	-3	-2	0	0	-4	0	0	-1	0	0	1	0	-3	-1	-2	1	-2
25.51	-1	0	-1	0	-1	0	1	0	1	0	2	0	3	2	2	3	4	4	1	2
125.56	2	1	0	0	-1	0	-2	0	2	0	0	2	2	1	4	5	2	2	2	4
225.61	-1	-1	0	1	0	1	0	-1	-1	-1	-2	0	1	0	1	1	1	1	2	2
325.66	0	-1	-1	0	0	-1	0	-2	-1	0	-2	-1	-1	0	0	1	1	1	-2	2
425.71	0	1	1	-2	0	-2	1	0	1	1	-2	-2	-2	0	-1	0	0	-1	2	0
525.76	-1	-1	-2	1	-1	1	0	2	0	2	0	-1	-2	-3	0	1	-1	0	-2	0
625.81	0	-1	2	-1	-1	0	0	0	1	1	0	-1	1	-3	-3	-1	-1	-2	-1	-1
725.85	1	0	0	0	1	-1	0	2	1	0	-2	1	1	-2	0	2	-2	-3	-4	-1
825.90	3	0	0	-1	1	2	1	0	-1	-1	-1	-1	0	-1	1	-2	0	-2	-2	-3
925.95	0	0	-1	-1	-1	1	-1	0	0	1	1	2	0	1	0	0	1	0	0	1

	$\mathrm{Im}\, b_{111}$																			
f′ f	25				226				326				526				726			926
-925.95	2	2	-3	3	2	0	1	0	-2	-1	1	0	1	0	1	-1	-1	0	1	0
-825.90	2	3	2	2	1	2	1	1	1	1	0	1	1	0	3	0	1	0	1	1
-725.85	2	2	4	3	1	3	2	-1	3	-1	-1	0	0	-1	0	0	2	-1	2	3
-625.81	2	4	5	4	3	2	3	0	2	1	0	0	0	2	0	0	1	1	0	1
-525.76	2	3	5	4	1	3	3	1	2	4	1	2	1	2	0	0	-2	-2	0	3
-425.71	2	4	6	5	3	3	3	3	1	2	1	2	3	0	1	2	1	2	1	2
-325.66	2	6	5	5	2	2	3	1	5	2	4	2	1	2	1	1	2	2		
-225.61	6	9	5	4	3	3	5	2	2	2	3	2	2	1	2	2	3	3	2	2
-125.56	6	7	5	6	5	5	4	5	3	6	6	5	2	4	2	3	2	4	0	3
-25.51	4	9	6	6	3	4	4	4	2	2	3	3	2	2	3	3	3	3	2	3
25.51	0	-6	-8	-7	-5	-3	-2	-3	-3	-3	0	0	-1	-1	0	-1	-3	-2	-2	-2
125.56	0	1	0	-7	-5	-5	-3	-2	-2	-5	-3	-3	-3	-2	-2	-2	-2	-1	1	-2
225.61	-1	-1	-2	0	0	-6	-4	-2	-2	-4	-4	-5	-4	-3	-3	-1	-3	0	0	-2
325.66	-1	1	2	[illegible]	-1	0	2	-4	-4	-4	-4	-5	-4	-2	-3	-1	-2	-1	-3	-2
425.71	0	-1	-2	-2	1	1	0	1	-1	-4	-3	-2	-2	-2	-2	-2	-1	-2	-1	0
525.76	-2	-2	0	0	-1	1	0	0	0	1	-2	-3	-3	-2	-3	-2	-1	-1	0	-2
625.81	1	1	0	0	0	0	-1	1	1	-1	1	0	0	0	-2	-1	-2	-2	-1	-2
725.85	-1	0	0	2	-1	1	-1	0	-1	2	1	0	0	-1	1	-1	-2	-1	0	-2
825.90	0	-1	-1	-1	1	3	0	2	-1	0	1	0	0	0	-1	1	3	-2	0	0
925.95	-1	0	1	-1	0	1	1	1	2	1	-1	0	0	0	-1	-2	-1	0	-1	-1
	$\mathrm{Im}\, b_{211}$																			
-925.95	0	2	2	2	1	0	2	0	1	0	0	2	0	-1	-1	1	0	1	0	0
-825.90	0	-1	1	1	0	2	0	0	-1	-1	-1	2	-1	-1	0	0	0	0	-1	2
-725.85	0	0	1	3	2	2	0	1	0	2	0	0	0	-1	0	1	1	1	-2	1
-625.81	-1	0	-1	0	1	1	0	0	0	1	-1	0	-2	2	1	0	-1	0	-1	-1
-525.76	0	-1	2	2	0	0	0	2	1	0	2	-1	0	1	0	1	0	0	2	2
-425.71	2	1	2	-1	-2	0	2	0	0	3	0	0	0	-1	1	0	0	1	-2	1
-325.66	1	1	1	-1	0	0	0	0	1	2	-1	-2	-1	-1	1	0	0	0	0	1
-225.61	0	1	1	0	-1	1	1	1	2	-1	2	2	3	0	0	-3	1	1	0	1
-125.56	0	0	0	0	0	0	0	1	1	0	1	1	1	1	0	0	0	1	2	2
-25.51	-1	-2	0	1	0	-1	1	3	2	1	1	1	1	1	0	1	0	2	2	2
25.51	-1	1	1	0	0	0	0	0	1	0	2	2	1	0	3	1	2	0	1	1
125.56	1	-1	1	-2	-1	0	2	-1	0	-1	3	0	1	0	1	1	1	0	1	1
225.61	0	0	-1	2	-1	1	1	1	0	-1	2	1	0	-1	-1	0	1	0	-2	1
325.66	2	-2	1	-1	2	-2	1	-1	1	0	2	1	1	-1	1	0	-1	2	2	1
425.71	0	1	0	-1	0	1	-1	2	1	-2	0	0	-1	1	1	0	-1	2	0	0
525.76	0	1	0	-1	0	-2	1	-3	-1	0	0	0	0	0	0	1	1	0	-1	2
625.81	0	0	0	0	0	1	0	-1	2	2	-1	0	0	1	0	1	-2	-1	0	-1
725.85	-2	-1	-1	0	0	0	0	0	0	-1	0	0	2	0	0	1	1	0	-1	1
825.90	-1	2	1	-1	0	1	1	-1	0	-1	0	-2	-2	-1	0	0	-2	0	1	1
925.95	0	-1	-1	0	0	-3	-1	1	1	1	0	0	0	2	-1	1	1	0	1	-1

Table 4. Resolvability of one-dimensional bispectra $b_{111}(f, f'; \bar{x}, \bar{x}', \bar{x}'')$ and $b_{211}(f, f'; \bar{x}, \bar{x}', \bar{x}'')$ for Case 5.2.

	Re b_{111}																			
f′ \ f	26				226				326				526				726			926
-925.95	0	1	1	1	-1	0	1	1	2	-2	1	1	1	1	0	0	2	0	0	-1
-825.90	-1	0	-1	2	-1	-1	1	0	1	-1	0	2	-1	-2	0	1	0	0	0	0
-725.85	-1	0	1	0	-1	-1	2	0	0	1	2	0	-1	1	-1	0	-2	-2	0	-2
-625.81	2	-1	1	0	-1	-2	0	1	0	0	0	-1	0	-1	0	1	1	0	2	-1
-525.76	1	-1	-1	1	0	-1	-1	0	0	1	1	0	1	0	0	-1	0	0	0	1
-425.71	-3	0	1	-1	0	-2	-1	0	0	-1	0	-2	0	-1	1	0	1	0	-1	-1
-325.66	0	0	0	0	2	0	0	0	0	1	1	1	0	0	-1	0	0	0	-1	-2
-225.61	-1	0	0	-1	-1	-1	1	0	-1	0	-1	1	0	2	0	1	-2	1	1	1
-125.56	0	1	-1	2	-1	1	-1	1	-1	-1	1	0	0	0	-2	0	0	1	0	1
-25.51	1	1	-1	1	2	0	1	0	-1	-1	0	-1	1	1	0	2	0	3	0	1
25.51	1	0	1	0	-1	-2	0	0	1	2	0	0	-1	-1	0	0	0	-1	1	0
125.56	-1	0	2	0	0	2	-1	0	0	2	0	1	1	0	0	0	0	0	1	-1
225.61	0	1	0	0	-3	-1	1	1	0	1	0	0	-1	1	-1	0	-1	1	0	-1
325.66	-1	1	-1	-1	1	0	0	0	-1	1	1	0	1	0	-1	0	-1	-1	0	-1
425.71	-2	0	0	1	-2	0	0	-2	0	-1	-1	1	0	2	0	2	-1	-1	1	0
525.76	1	1	1	0	0	-1	2	0	-1	1	1	-1	0	0	1	2	0	-1	-1	1
625.81	1	0	0	-1	1	1	-1	0	-1	1	0	0	-2	-1	0	-1	-2	-1	2	-1
725.85	0	-1	1	2	1	-1	1	0	-1	1	0	-1	0	0	1	1	0	-1	-2	0
825.90	1	1	-1	0	0	1	2	-2	1	0	1	1	0	-2	2	1	0	-1	-1	1
925.95	0	-1	0	-1	-1	1	-1	0	-1	0	0	-1	-1	0	0	1	-1	-2	1	0

	Im b_{111}																			
f′ \ f	26				226				326				526				726			926
-925.95	0	0	-1	1	2	0	0	1	0	-2	-1	1	-2	1	0	0	-1	-1	1	0
-825.90	0	1	2	0	-1	-1	1	-1	1	0	1	1	1	0	-1	0	0	2	1	-1
-725.85	0	0	0	0	0	-1	0	0	1	-1	0	-1	0	-1	0	-2	1	0	0	1
-625.81	0	2	1	-1	-1	1	-1	-1	-1	0	0	0	-1	0	0	-1	2	1	-2	0
-525.76	-3	0	1	-1	-2	0	1	-1	-1	1	1	0	0	1	0	2	0	-1	1	0
-425.71	-1	-1	-1	1	0	-1	0	1	-1	0	1	0	0	0	3	1	0	-1	0	0
-325.66	0	0	-1	0	0	0	-1	2	2	0	-2	-2	-1	-1	-1	-2	-1	-1	1	0
-225.61	-1	0	0	2	-1	1	0	2	1	1	-1	0	1	0	2	1	-1	-1	0	1
-125.56	0	2	1	1	0	0	-2	1	0	-3	0	-1	1	0	1	-1	2	0	0	-1
-25.51	4	3	0	-1	-1	0	0	-1	1	-1	0	0	-1	0	1	0	-1	-1	1	-2
25.51	1	-2	-1	-1	2	1	0	0	0	1	0	-1	1	-1	0	0	1	1	2	-1
125.56	0	0	1	1	1	-1	-1	0	0	1	-1	2	0	-3	0	-2	1	1	0	-2
225.61	-1	1	-2	-1	0	1	0	1	1	-2	2	1	1	0	0	1	-2	1	0	1
325.66	1	0	0	1	1	-2	1	1	0	1	0	0	1	0	0	-1	1	0	0	1
425.71	0	0	0	-1	0	0	-1	0	1	1	2	0	0	0	0	1	0	0	-1	-1
525.76	0	-1	0	1	0	-2	0	-3	1	0	0	0	-1	-1	1	0	-1	-2	0	1
625.81	0	0	-1	-1	-1	-1	-2	-1	-2	0	0	0	0	0	0	0	2	0	-1	-1
725.85	0	-1	0	0	1	0	-1	0	0	-1	1	0	-1	0	2	-1	-1	-1	0	0
825.90	-1	0	1	0	0	-1	0	1	0	0	2	1	-1	0	0	1	1	-1	1	0
925.95	-1	0	2	0	0	1	-1	-1	0	-1	0	-1	-1	-1	0	-1	-1	2	-1	0

	Re b_{211}																			
f′ \ f	26				226				326				526				726			926
-925.95	0	-1	0	-2	1	0	2	0	0	2	0	-1	0	-1	1	0	2	1	0	-1
-825.90	1	-1	-1	1	1	0	0	-1	-1	0	-1	-1	0	0	1	1	-1	0	0	-2
-725.85	1	0	-1	0	1	0	1	0	-1	1	0	-1	0	1	0	0	0	1	-1	-2
-625.81	-1	1	-1	1	2	0	0	-1	0	-1	1	0	1	1	0	2	0	0	-2	3
-525.76	0	-1	0	-1	-1	0	0	2	-1	1	1	1	1	0	1	1	1	1	0	1
-425.71	-1	0	-1	0	1	0	-1	0	1	1	1	-1	-1	1	0	-1	0	1	0	1
-325.66	2	-1	1	-2	0	-1	-1	-1	-2	1	0	2	0	-1	1	0	0	1	1	1
-225.61	-1	1	-2	1	1	-1	0	0	2	1	-1	0	0	0	-1	1	1	0	-1	0
-125.56	0	0	1	0	0	0	0	0	0	-1	1	1	0	-1	0	-1	-1	2	1	1
-25.51	1	1	0	-1	1	0	-2	1	0	0	-2	-1	0	-1	-1	-1	-1	-2	-2	0
25.51	3	1	2	3	-2	1	0	2	0	2	0	0	3	2	2	1	-1	1	-2	1
125.56	1	0	1	1	1	-1	0	1	0	-1	-2	0	1	-2	1	1	-1	2	0	-1
225.61	1	1	0	2	0	1	0	0	-1	-1	1	0	0	0	1	0	-1	0	1	-1
325.66	1	0	2	-1	0	0	0	0	0	0	1	0	0	1	1	-1	1	1	0	0
425.71	0	0	0	1	1	-1	1	1	2	1	0	-2	0	0	0	-1	1	1	0	-1
525.76	-1	-1	0	-1	0	1	0	1	1	0	-1	1	1	-1	1	1	0	0	1	0
625.81	0	1	-1	-2	-1	0	1	-1	1	0	2	1	-2	-1	0	1	0	0	-1	0
725.85	-1	0	1	-3	-2	0	1	2	1	1	-1	0	1	0	0	-1	2	0	-1	0
825.90	0	0	2	-1	-1	-1	0	-1	-2	0	0	1	-2	1	2	0	0	0	0	0
925.95	0	0	1	1	0	-1	0	-1	0	-1	-1	-1	0	0	0	-2	2	0	0	-1

	Im b_{211}																			
f′ \ f	26				226				326				526				726			926
-925.95	-2	1	0	1	1	-1	1	-1	0	1	0	1	-1	1	-1	0	1	-1	0	-1
-825.90	1	0	0	-2	2	-1	-1	0	-2	2	1	-1	0	-1	0	1	1	0	0	0
-725.85	1	-1	-2	0	0	1	-1	0	-1	1	-2	1	2	-1	2	0	1	1	1	2
-625.81	1	1	1	1	-4	0	0	0	2	1	1	1	0	-1	-1	1	0	0	-1	1
-525.76	-2	0	-1	2	0	1	-1	-1	-1	-1	0	0	2	-1	-1	0	0	0	1	1
-425.71	0	0	0	0	0	0	1	0	1	0	0	0	0	0	3	-1	1	-1	0	0
-325.66	0	-1	0	0	0	-1	0	0	0	-1	0	-1	0	1	0	-1	0	-1	2	0
-225.61	1	-1	2	0	1	-2	1	0	1	0	0	-1	1	1	0	-1	-1	1	1	-1
-125.56	1	0	-2	0	0	-1	2	2	1	0	0	1	-1	-1	0	1	1	0	0	2
-25.51	0	1	-2	1	0	0	2	-1	1	0	0	1	-1	-1	1	1	0	1	0	-1
25.51	2	0	1	2	0	1	0	0	2	1	0	-1	2	-1	0	0	0	-1	1	-1
125.56	-1	1	1	-1	2	0	0	-2	-1	0	2	-1	0	1	-1	1	0	0	1	2
225.61	0	0	0	-2	0	1	1	-3	-1	-1	0	-1	1	0	1	3	-1	-1	0	0
325.66	-1	-1	0	-1	0	0	-1	0	1	0	0	1	0	0	0	0	1	2	-1	-2
425.71	1	1	-2	0	0	2	0	1	-2	-2	1	1	0	0	0	1	-2	0	0	0
525.76	0	0	2	-1	0	1	0	1	-1	-1	-1	1	-1	0	1	0	-2	1	3	0
625.81	0	1	-1	0	0	0	0	-1	0	1	0	2	-1	-1	-1	0	0	0	1	2
725.85	0	-1	-1	0	0	1	-2	2	-3	0	0	-1	-1	-3	1	-1	-1	-1	1	-1
825.90	1	0	-1	0	0	0	0	0	-1	1	0	1	0	0	0	0	1	1	1	-2
925.95	0	0	0	0	-2	0	1	0	-1	0	-1	3	0	1	-1	-1	0	0	-1	-1

Table 5. Resolvability of one-dimensional bispectra $b_{111}(f, f'; \bar{x}, \bar{x}', \bar{x}'')$ and $b_{211}(f, f'; \bar{x}, \bar{x}', \bar{x}'')$ for Case 8.4.

	Re b_{111}																			
f' f	26				226				326				526				726			926
-926.95	2	2	0	-1	-1	1	-2	0	2	1	0	0	-1	0	-1	-1	0	1	2	-2
-826.90	1	-1	-1	-1	0	-1	0	0	0	1	-1	0	-1	1	-1	0	1	0	1	0
-726.85	0	-1	-1	0	-2	-1	1	-1	0	-1	-2	1	-1	1	-1	0	-1	0	-1	0
-626.81	-1	1	0	0	1	0	1	2	-1	1	0	1	0	1	-1	0	-2	-1	-1	0
-526.76	-1	0	0	-1	-1	0	1	0	-1	1	0	2	0	1	0	0	0	1	0	0
-426.71	-1	0	-3	-1	0	0	0	-1	0	1	-1	2	-1	1	0	1	1	2	1	1
-326.66	1	-1	1	0	1	0	0	1	0	1	-1	0	1	0	1	-1	0	0	-1	0
-226.61	0	0	1	0	-1	0	1	0	0	1	0	1	1	0	-1	0	0	-1	-1	0
-126.56	-1	-1	-1	1	1	-2	1	0	-3	-1	0	-2	-2	1	0	1	-1	2	0	-1
-26.51	0	1	-1	0	-1	1	0	2	0	2	-2	2	1	0	0	-3	0	0	1	1
26.51	-2	1	-1	1	2	2	0	0	-1	1	-1	0	-1	-3	-1	1	0	2	-1	0
126.56	-1	0	-1	-1	0	0	1	-1	1	1	1	0	0	1	1	0	1	-1	1	-1
226.61	0	-1	1	-1	2	1	0	0	0	0	0	1	-2	-2	0	-1	1	-1	0	1
326.66	-1	-1	1	0	0	0	1	1	-2	0	1	1	0	-1	1	0	-3	-1	1	-1
426.71	1	1	-1	0	0	1	0	-1	1	0	0	-1	0	1	1	2	-1	0	-1	-1
526.76	0	1	1	0	1	1	0	0	[illegible]	0	0	0	-2	0	-1	-1	3	2	-1	0
626.81	1	0	0	-1	0	1	1	0	1	0	-3	1	2	0	0	1	0	0	2	1
726.85	2	-1	1	1	0	-1	2	0	0	1	2	-1	1	-2	1	0	-2	-1	0	0
826.90	-1	0	1	1	0	0	0	0	-2	0	1	0	0	-2	-1	-1	-1	0	-1	1
926.95	-1	0	-1	0	-1	-1	1	0	-1	0	0	0	0	2	0	-1	0	0	-1	1

	Im b_{111}																			
f' f	26				226				326				526				726			926
-926.95	-1	1	0	-1	-1	-1	-1	0	0	0	-1	1	1	1	0	2	1	-1	-1	-1
-826.90	1	0	1	1	2	1	0	1	3	1	1	1	0	2	1	2	-1	-1	1	1
-726.85	2	2	-1	0	-1	0	0	0	0	0	0	-2	-1	0	-2	-1	1	0	1	-1
-626.81	-2	0	2	1	0	1	1	1	0	-1	-1	-1	1	1	-1	1	-1	0	0	1
-526.76	1	0	1	-2	1	1	1	-1	1	0	-2	2	0	-1	-2	-1	1	-1	0	0
-426.71	-1	0	0	0	-1	0	0	0	0	-1	0	0	1	-1	-1	1	1	0	1	0
-326.66	1	-1	-1	1	0	-1	0	-1	0	0	1	-1	1	1	-1	-1	-1	0	-1	1
-226.61	-1	1	0	1	0	-1	0	-1	-1	1	1	0	0	-1	1	-1	3	0	-1	0
-126.56	0	0	-1	-1	0	1	-1	-2	0	-1	0	-1	0	-1	0	1	-1	2	0	-1
-26.51	-2	0	0	0	0	1	1	0	-1	-1	-1	1	-2	1	0	0	1	-1	1	0
26.51	1	-2	1	-2	1	1	1	0	-1	0	-1	-3	0	1	-2	1	0	2	-1	-1
126.56	2	0	1	-1	0	0	-2	0	0	-1	-1	-1	0	-1	1	-1	-1	0	0	-1
226.61	-1	2	1	0	1	-1	2	-2	-1	0	2	0	-1	1	0	-2	2	0	0	-1
326.66	1	1	0	-2	0	1	1	0	0	3	2	-1	0	0	-1	0	0	1	0	1
426.71	1	1	-1	1	1	-1	0	1	2	2	-1	1	-2	0	0	0	0	0	0	2
526.76	-1	-1	0	-1	-1	0	-1	1	-1	0	0	-2	0	1	-1	0	-1	0	1	1
626.81	2	-2	0	0	1	0	0	-1	0	0	-1	1	2	0	0	1	2	-1	0	0
726.85	0	0	1	0	-1	1	0	1	0	-1	0	1	-2	0	0	0	0	-1	-1	3
826.90	-3	1	-1	0	1	0	0	-1	1	-2	-1	0	0	0	1	0	2	1	0	0
926.95	1	2	1	0	1	0	1	-1	0	-2	-1	0	0	0	-2	0	0	0	2	-1

	Re b_{211}																			
-926.95	1	0	2	1	-1	-1	2	0	0	2	-1	0	1	0	0	-2	0	1	1	0
-826.90	0	0	3	-1	1	1	-2	-1	1	1	1	1	0	-1	0	-1	1	-1	-1	0
-726.85	0	0	-1	0	-1	-2	0	1	0	1	-1	0	1	-1	1	-2	1	-1	2	0
-626.81	0	-1	0	1	-1	1	-1	-1	0	1	-2	1	1	0	0	1	0	-1	1	1
-526.76	-1	1	0	0	0	1	0	-1	0	0	1	-2	-2	1	-2	0	2	1	-1	0
-426.71	-1	1	0	-1	0	-1	-1	-1	1	1	-1	-1	0	1	0	0	0	-1	0	0
-326.66	0	1	-1	-1	-1	-1	1	-1	-1	1	1	1	0	-1	0	2	1	1	0	1
-226.61	1	1	0	-1	0	-1	0	-1	0	-1	1	-1	-2	-1	-2	1	0	1	0	0
-126.56	-1	1	0	0	-1	1	-1	1	0	1	-1	0	-1	0	-2	0	1	0	0	0
-26.51	1	-1	-1	-1	1	0	0	2	0	0	-1	-1	-1	0	0	1	-1	0	0	2
26.51	2	1	2	0	-2	0	0	-1	-1	0	1	-1	0	-1	-1	0	-1	1	0	0
126.56	1	0	0	2	1	-1	0	0	2	1	-1	-1	1	2	1	1	1	0	1	1
226.61	3	-2	0	-1	-2	2	1	1	-1	-2	-2	0	1	1	0	2	0	0	1	1
326.66	1	1	0	1	1	-1	1	0	2	0	-2	0	0	0	-1	1	0	0	-1	1
426.71	-1	0	-1	0	-1	1	1	0	1	2	1	1	0	-1	0	0	-2	0	-1	1
526.76	0	-1	0	0	1	-2	0	1	0	2	-1	2	1	1	0	-1	-1	-1	0	1
626.81	2	1	-1	0	0	-1	0	0	0	-2	0	-1	0	-1	0	1	-2	0	-1	0
726.85	0	0	1	0	1	-1	0	1	0	-2	0	1	-1	1	2	1	-2	2	1	-1
826.90	0	-1	2	0	-1	1	-2	0	0	0	0	1	-1	-1	-2	-2	0	1	0	2
926.95	0	1	0	1	2	-1	2	-1	1	-1	2	-1	1	1	-1	0	-2	0	1	-1

	Im b_{211}																			
-926.95	2	0	-1	-1	1	-2	1	0	0	-1	0	0	-2	-1	-1	0	0	-2	1	-1
-826.90	0	-1	1	0	0	-1	0	2	-2	1	-1	1	1	0	0	-2	0	-1	0	-2
-726.85	0	1	1	2	-1	0	0	0	0	-2	1	-1	1	-1	0	1	1	0	-1	0
-626.81	0	0	-1	-1	0	-1	0	0	-1	-1	0	-1	0	-1	0	1	0	0	-2	0
-526.76	2	0	3	-1	-1	2	1	-2	0	2	0	0	0	0	0	0	1	1	-1	-1
-426.71	0	0	-1	1	1	1	1	1	-1	0	-1	0	0	0	0	-3	0	1	0	-1
-326.66	0	1	1	-1	0	2	0	1	0	-1	1	2	0	-3	-2	1	0	-1	1	1
-226.61	1	0	0	1	1	0	0	0	1	-1	1	0	-1	1	-2	0	1	-1	0	2
-126.56	1	0	0	2	-1	-2	0	0	-1	0	1	-1	0	1	1	0	2	0	0	0
-26.51	-1	2	1	0	1	2	0	0	-1	0	0	-2	1	1	0	-2	0	-2	1	1
26.51	0	1	-1	0	-1	0	0	0	0	1	1	-1	-1	-2	-2	1	1	0	0	1
126.56	-1	0	1	1	2	0	0	1	-1	1	0	-1	1	-1	1	0	-1	1	-1	0
226.61	-2	1	0	2	0	1	0	-1	-1	-1	-1	0	-1	0	1	1	1	-2	-1	1
326.66	1	0	0	1	1	1	0	0	1	-1	-1	-1	-1	2	0	1	0	-2	-1	0
426.71	0	0	0	0	1	0	-2	1	0	1	0	1	0	-1	-1	-1	0	0	2	0
526.76	1	-1	0	2	-1	0	0	1	-1	0	-1	2	1	-1	1	1	-1	0	1	0
626.81	2	-1	-2	0	0	0	1	-1	1	3	2	1	0	0	1	0	-1	1	0	1
726.85	0	0	0	-1	1	1	0	1	-1	0	2	0	0	1	2	0	1	1	1	0
826.90	1	-1	1	0	0	0	0	0	-1	-1	0	-1	1	0	1	-2	0	0	1	0
926.95	-1	-1	0	-1	0	0	-1	0	1	-2	-1	2	1	0	1	0	0	1	-1	0

Table 6. Three-dimensional energy transfer spectrum Q(f, f′) representing the net energy transfer from spherical shell of radius f′ to the spherical shell of radius f. The standard deviations of the estimate Q is shown in parentheses.

f′ \ f	150	200	250	300	350	400	450	500	550	600
100	-11151 (3750)	312 (3000)	6812 (920)	8553 (3879)	3724 (1832)	-1112 (5312)	1010 (2520)	9690 (9900)	17897 (3078)	14340 (4630)
150	13028 (4590)	-13020 (8100)	-8213 (2266)	5550 (8100)	16144 (3214)	15768 (10980)	21917 (3492)	16283 (9000)	9141 (4399)	3298 (7551)
200	-12600 (5100)	-23000 (7600)	-13985 (2148)	1481 (1794)	17962 (4304)	28936 (16000)	24462 (5780)	5760 (20000)	-12936 (6256)	-17412 (7398)
250	-6375 (6000)	-17875 (7700)	-16287 (2986)	-949 (2175)	10544 (4832)	13220 (4520)	10160 (6897)	7712 (25000)	-22687 (7965)	-26475 (7219)
300	1980 (7200)	-8070 (7446)	-10740 (6375)	-6120 (11070)	1026 (4662)	1423 (19152)	-4971 (7086)	-6450 (3270)	-13358 (7841)	-18900 (7196)
350	5917 (6625)	-3010 (6650)	-7787 (3937)	-7770 (9450)	-5432 (3586)	-5971 (4126)	-3857 (4297)	6925 (4527)	8539 (8254)	-5084 (7468)
400	3480 (6000)	-3600 (5600)	-8600 (4000)	-5076 (2546)	-9520 (10920)	1252 (6442)	7812 (7200)	21000 (24000)	21558 (11092)	-1260 (9948)
450	-1620 (5400)	-5400 (6300)	-7537 (7875)	-9855 (9720)	-9450 (10868)	-5760 (13680)	9082 (5607)	20324 (8795)	12536 (12254)	-9680 (12101)
500	-3750 (4500)	-4400 (7800)	-3500 (7500)	-4350 (7200)	-5250 (9800)	-5600 (14000)	-1278 (5103)	2075 (27775)	-13384 (13970)	-20658 (15669)
550	-1073 (1790)	1410 (2793)	541 (3589)	785 (2856)	-3659 (4897)	-11310 (5350)	-16503 (4673)	-24398 (6424)	-23320 (12463)	-16946 (15724)
600	2682 (2115)	720 (6000)	1862 (3882)	-941 (4500)	-5405 (7079)	-6384 (29040)	-23744 (7171)	-6930 (26730)	23638 (8164)	-1022 (12078)
650	2564 (1804)	7683 (2509)	5952 (4001)	157 (6098)	-5000 (6466)	-11372 (2660)	-17000 (7596)	-17215 (9435)	-5963 (8455)	13112 (11790)
700	-2184 (1575)	3657 (1820)	6344 (3664)	1412 (12600)	-2268 (5334)	-2800 (17920)	-2591 (6662)	1680 (31150)	9028 (11007)	13474 (14616)
800	-7200 (1752)	-3131 (2362)	4976 (3220)	4200 (16320)	3716 (5527)	-401 (8506)	88 (11200)	6480 (33200)	2468 (16650)	-12653 (19349)

Table 7. Resolvability of the three-dimensional energy transfer spectrum.

f f′	150	200	250	300	350	400	450	500	550	600
100	-3	0	7	2	2	-0	0	1	6	3
150	3	-2	-4	1	5	1	6	2	2	0
200	-2	-3	-7	1	4	2	4	0	-2	-2
250	-1	-2	-5	-0	2	3	1	0	-3	-4
300	0	-1	-2	-1	0	0	-1	-2	-2	-3
350	1	-0	-2	-1	-2	-1	-1	2	1	-1
400	1	-1	-2	-2	-1	0	1	1	2	-0
450	-0	-1	-1	-1	-1	-0	2	2	1	-1
500	-1	-1	-0	-1	-1	-0	-0	0	-1	-1
550	-1	1	0	0	-1	-2	-4	-4	-2	-1
600	1	0	0	-0	-1	-0	-3	-0	3	-0
650	1	3	1	0	-1	-4	-2	-2	-1	1
700	-1	2	2	0	-0	-0	-0	0	1	1
800	-4	-1	2	0	1	-0	0	0	0	-1
900	0	1	1	-0	-2	-1	-1	-0	-1	-2

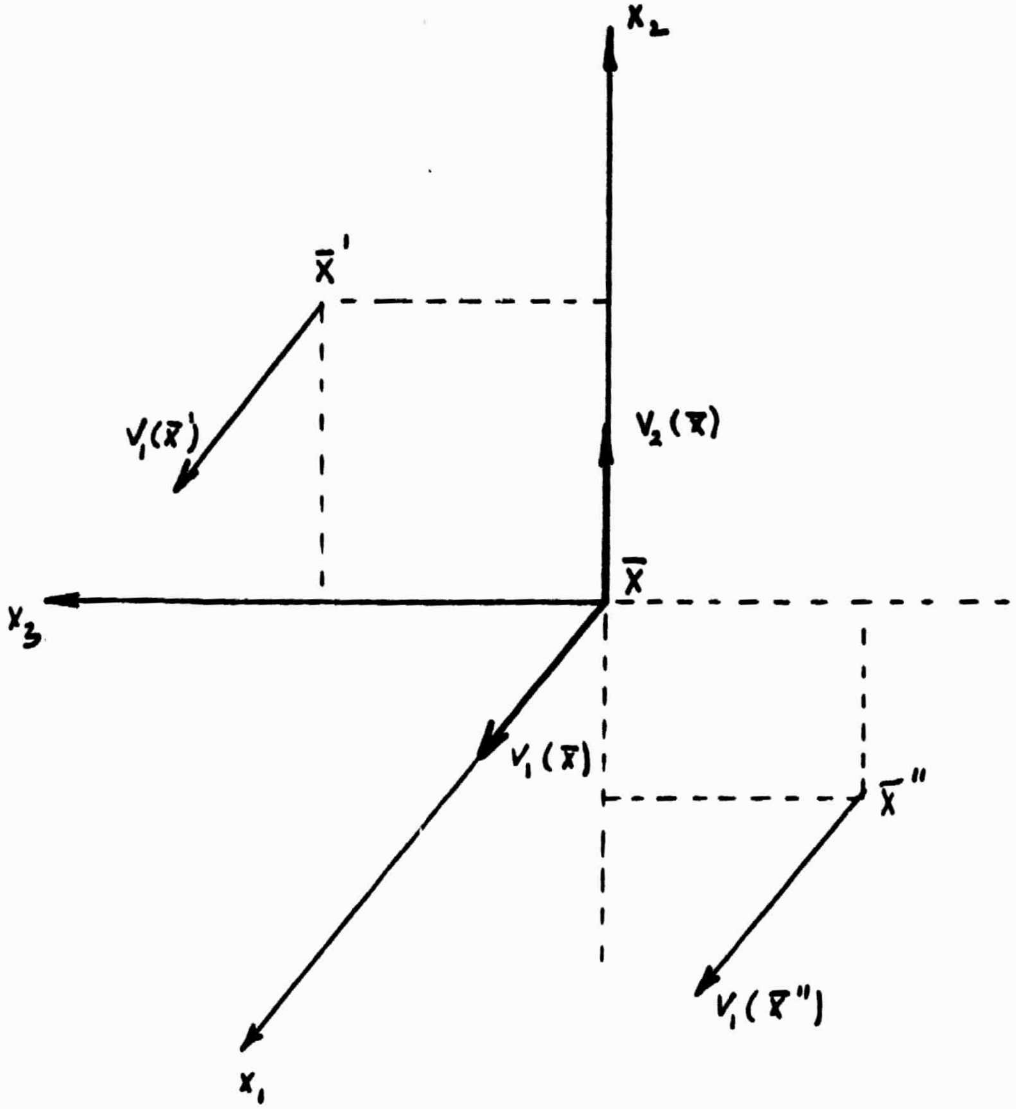

Fig. 1. Coordinate system for velocity sensors. The x_1 axis is pointed in the downstream flow direction.

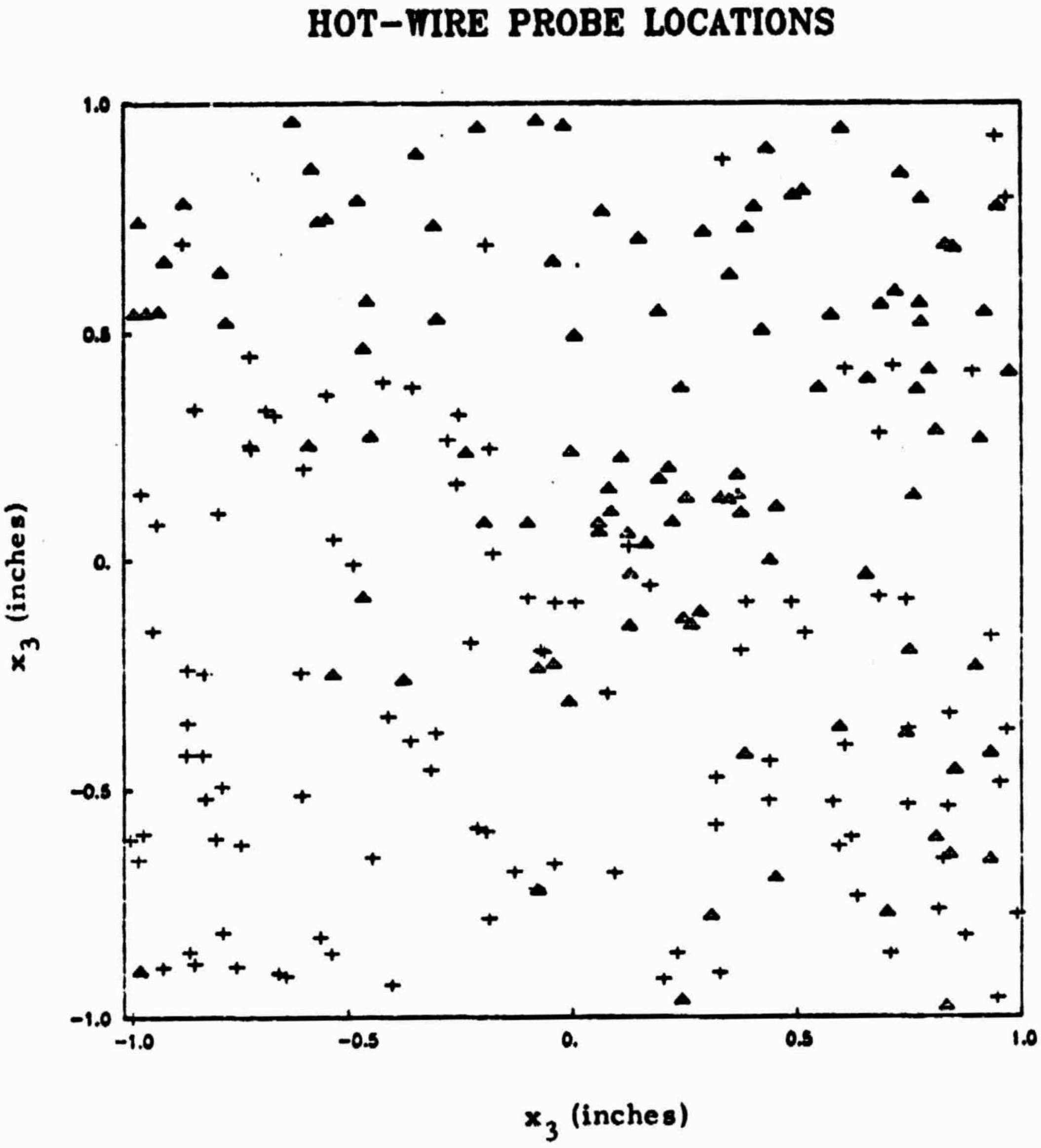

Fig. 2. Locations of the $\overline{x}'$ and $\overline{x}''$ velocity sensors (see Fig. 1).
+ is the $\overline{x}'$ sensor; Δ is the $\overline{x}''$ sensor.

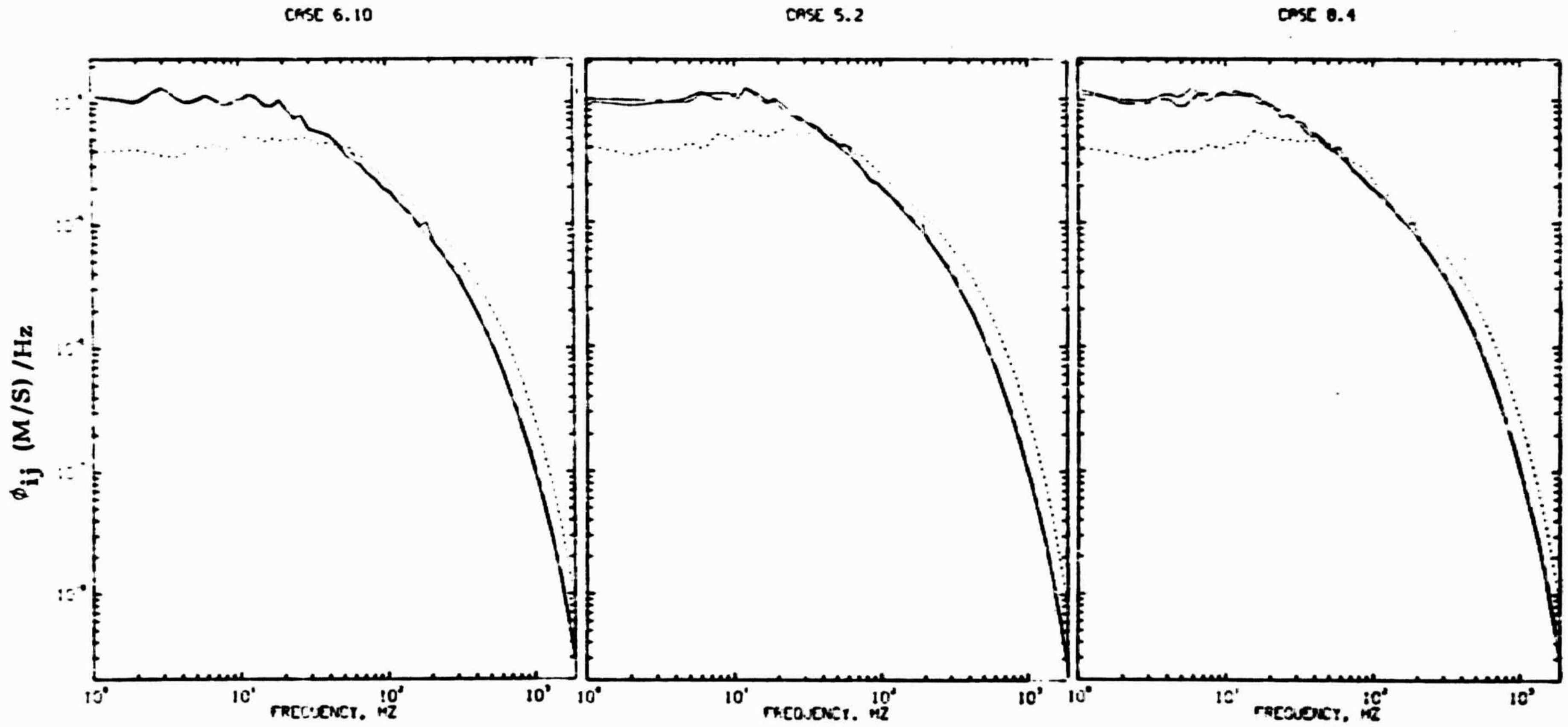

Fig. 3. One-dimensional energy spectra at selected locations given in Table 1. ———, $\phi_{11}(f;\bar{x})$; ------, $\phi_{22}(f;\bar{x})$; — — —, $\phi_{11}(f;\bar{x}')$; —·—, $\phi_{11}(f;\bar{x}'')$.

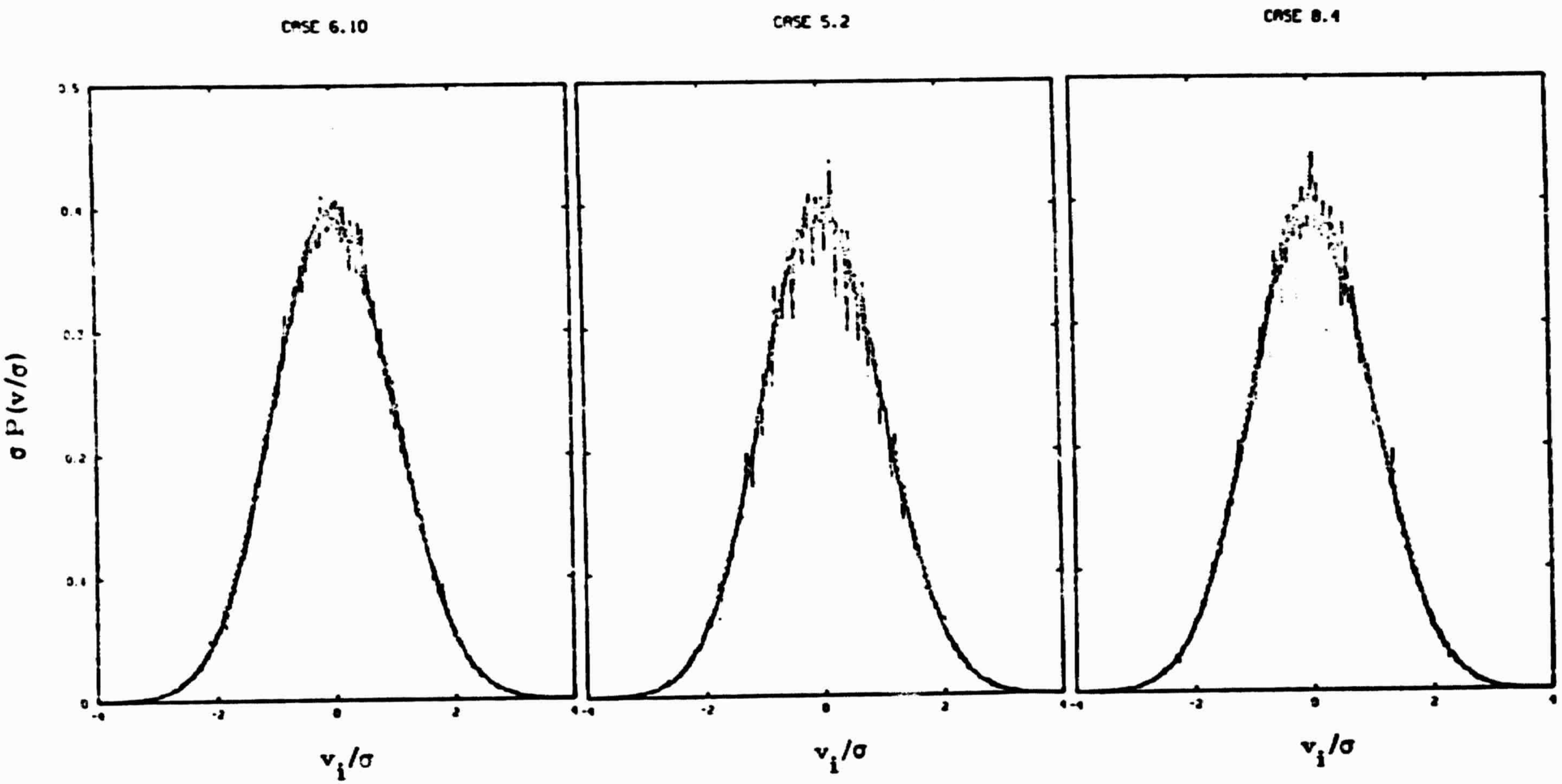

Fig. 4. Normalized probability density at selected locations given in Table 1 and σ = var(v).
———, $P[v_1(\bar{x})]$; - - - - - -, $P[v_2(\bar{x})]$; — - —, $P[v_1(\bar{x}')]$; — · —, $P[v_1(\bar{x}'')]$.

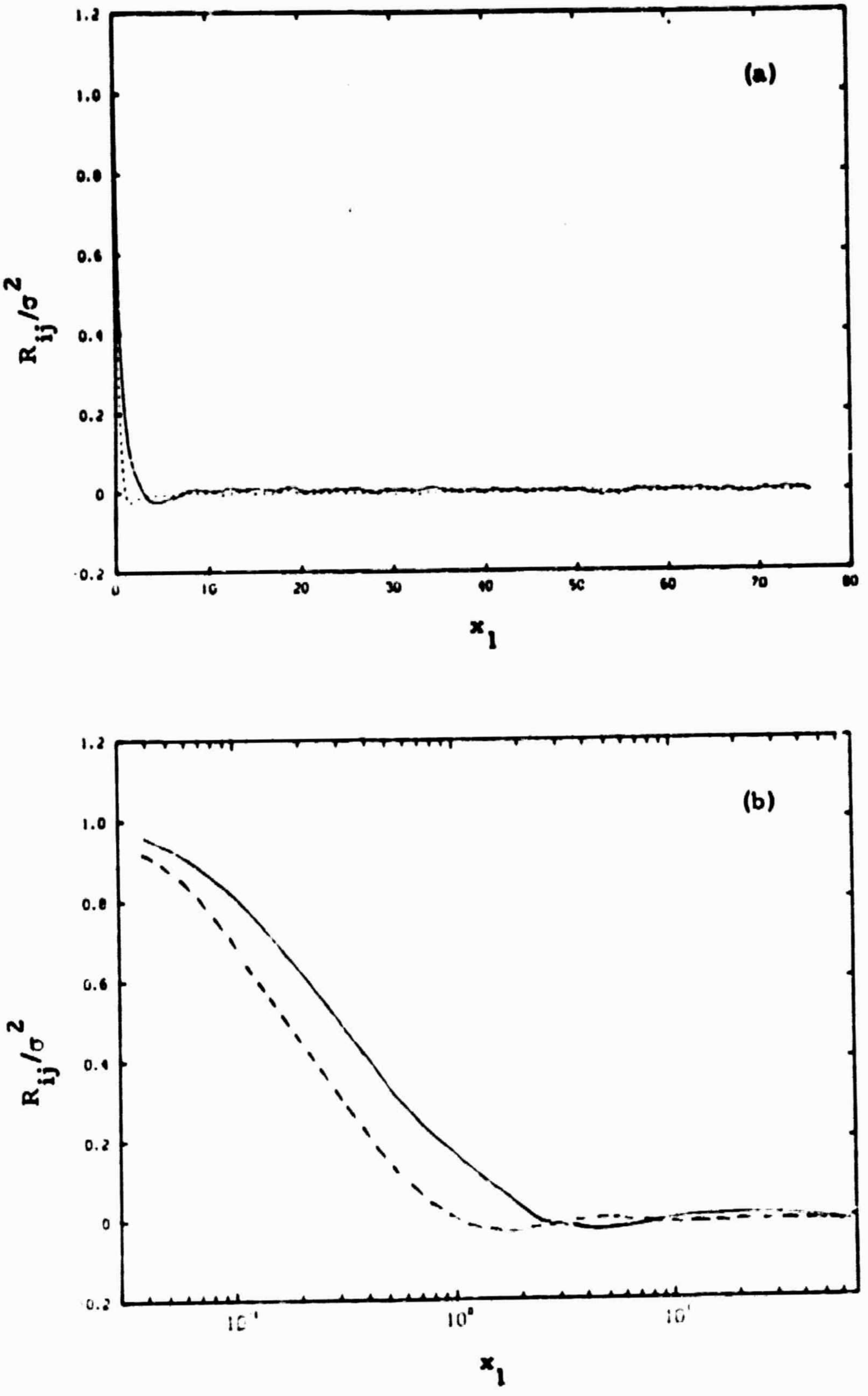

Fig. 5. Autocorrelations of $v_1(\bar{x})$ and $v_2(\bar{x})$ at location 4.10 given in Table 1. ———, $R_{11}(x)$; - - - - - -, $R_{22}(x)$. (a) Linear scale; (b) semi-logarithmic scale.

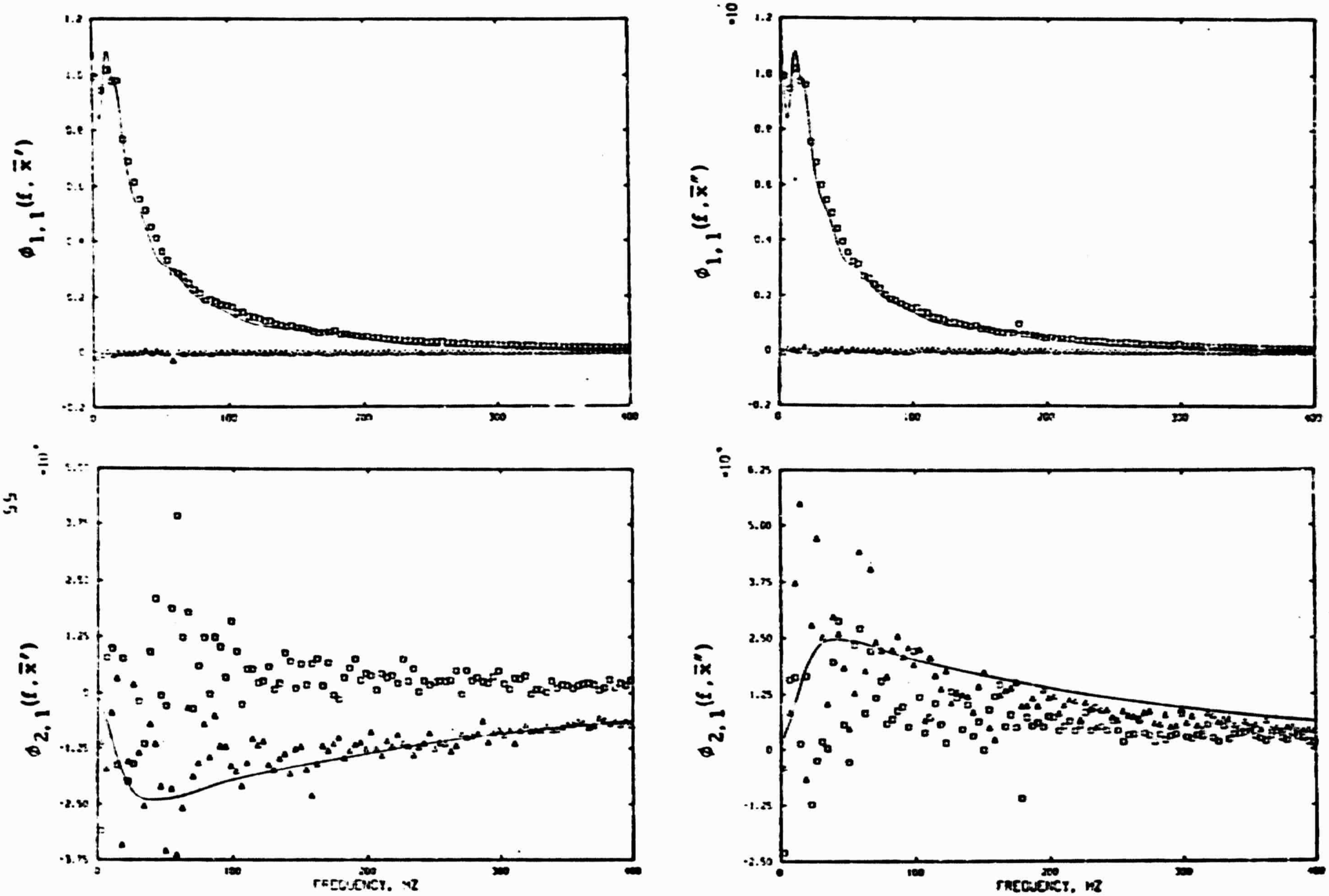

Fig. 6. Comparison of experimental and derived cross spectra for Case 6.10. □ , Experimental real part; Δ , experimental imaginary part; ———— , theoretical spectrum derived from autocorrelations of Fig. 5 using isotropy.

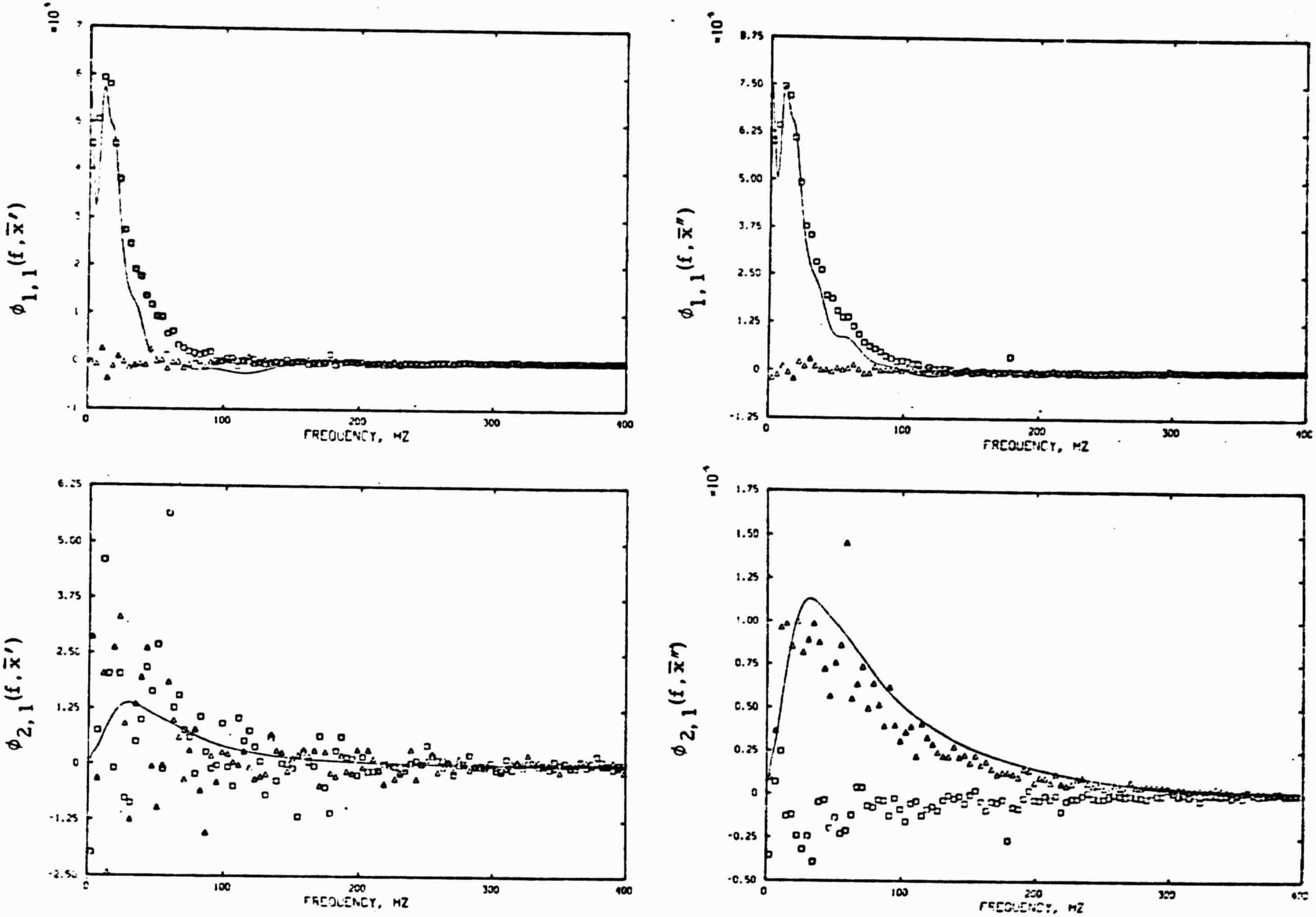

Fig. 7. Comparison of experimental and theoretical cross spectra for Case 5.2. □ , Experimental real part; Δ , experimental imaginary part; ——— , theoretical spectra derived from autocorrelations of Fig. 5 using isotropy.

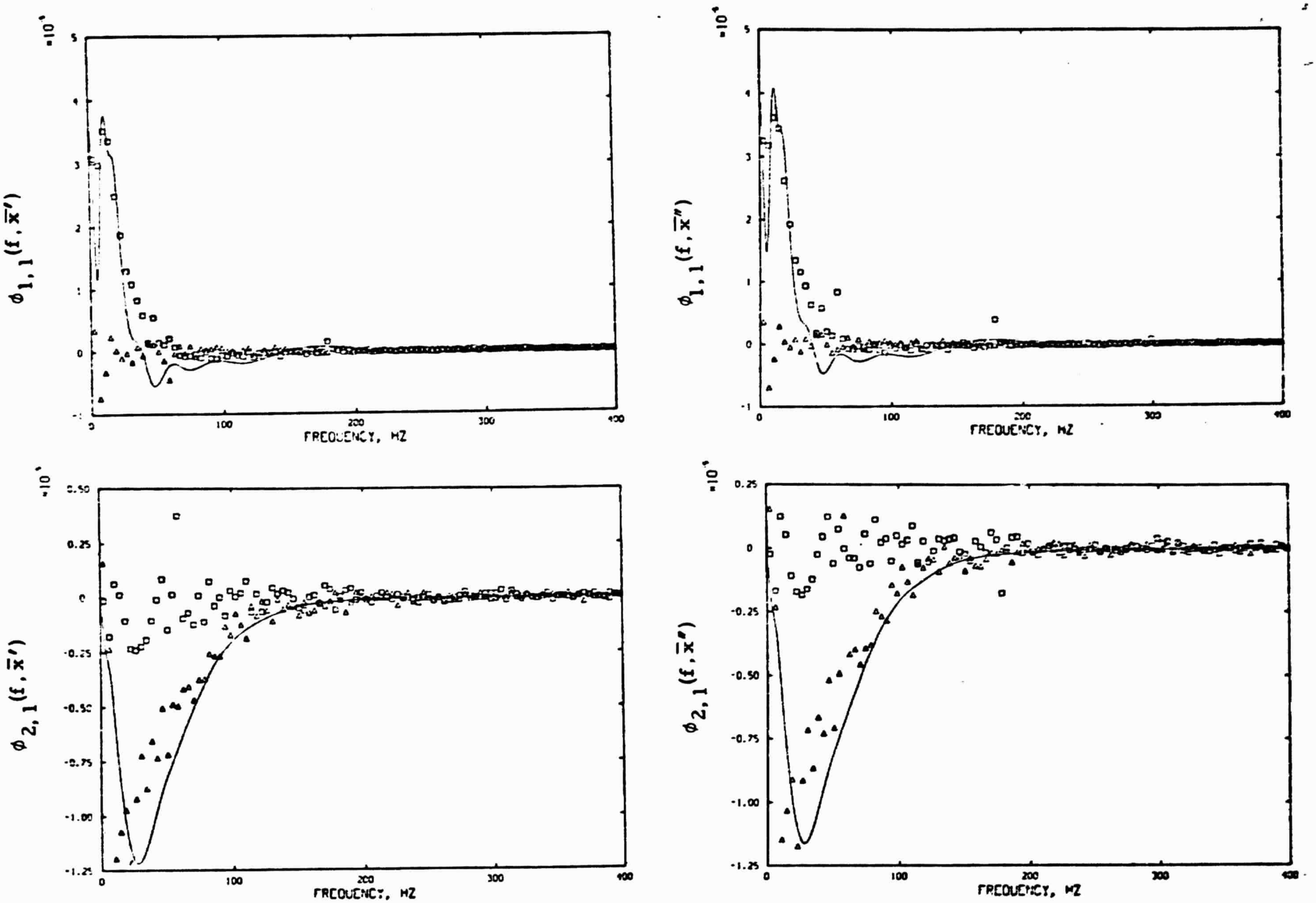

Fig. 8. Comparison of experimental and theoretical cross spectra for Case 8.4. ☐ , Experimental real part; △ , experimental imaginary part; ——— theoretical spectrum derived from autocorrelations of Fig. 5 using isotropy.

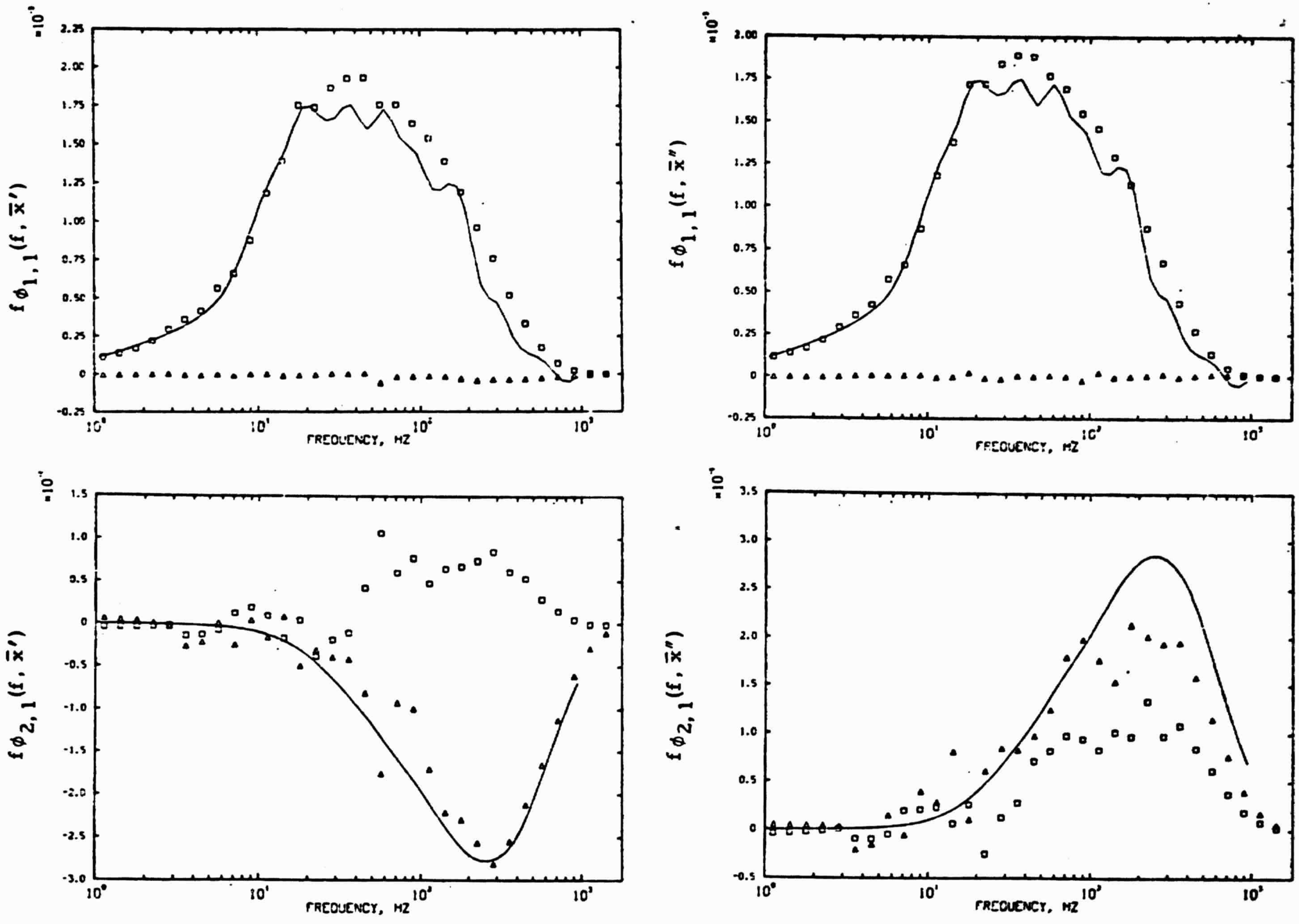

Fig. 9. Comparison of experimental and derived cross spectra for Case 6.10. □ , Experimental real part; Δ , experimental imaginary part; ———— , theoretical spectrum derived from autocorrelations of Fig. 5 using isotropy.

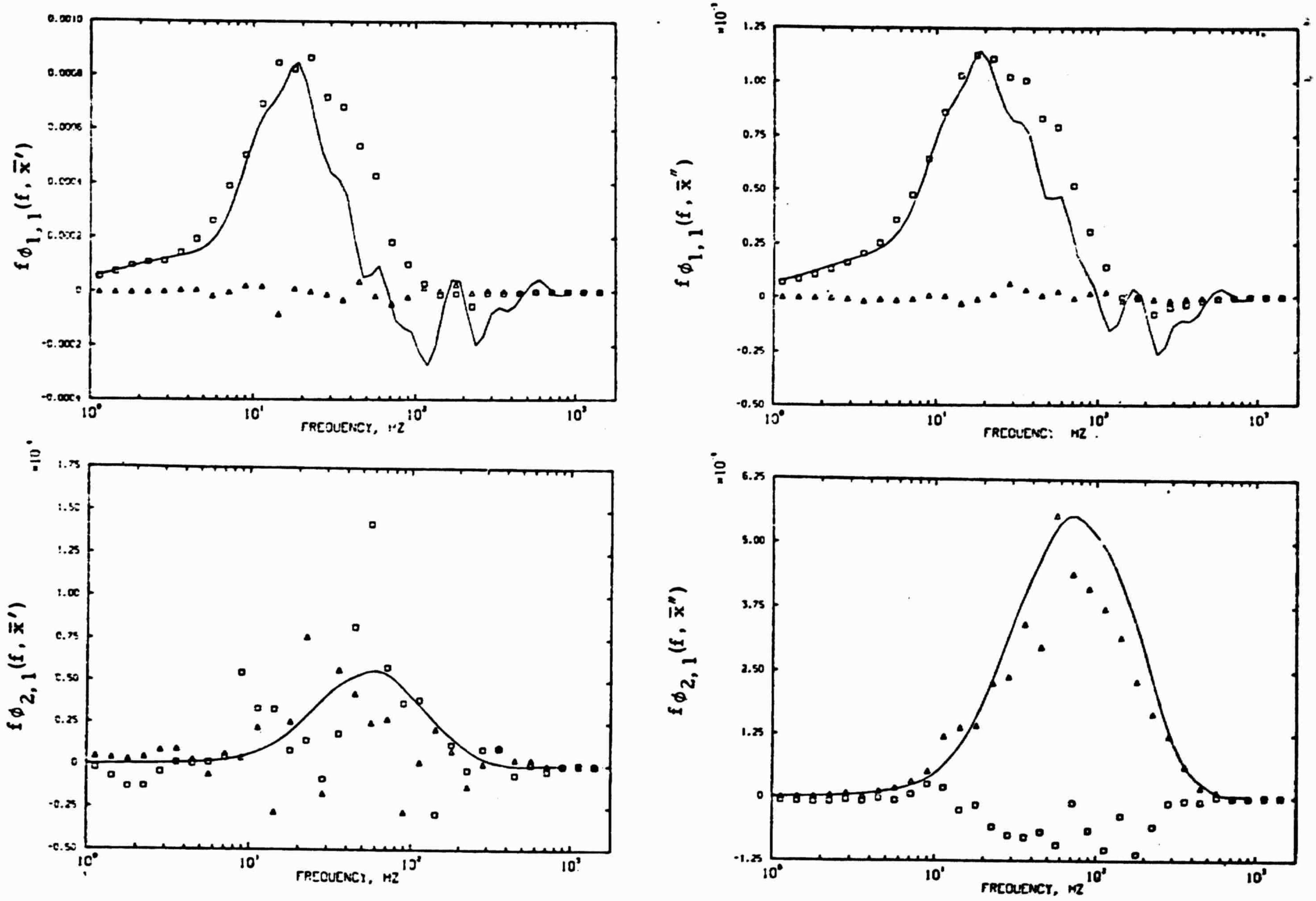

Fig. 10. Comparison of experimental and theoretical cross spectra for Case 5. 2. □ , Experimental real part; Δ , experimental imaginary part; ——— , theoretical spectra derived from autocorrelations of Fig. 5 using isotropy.

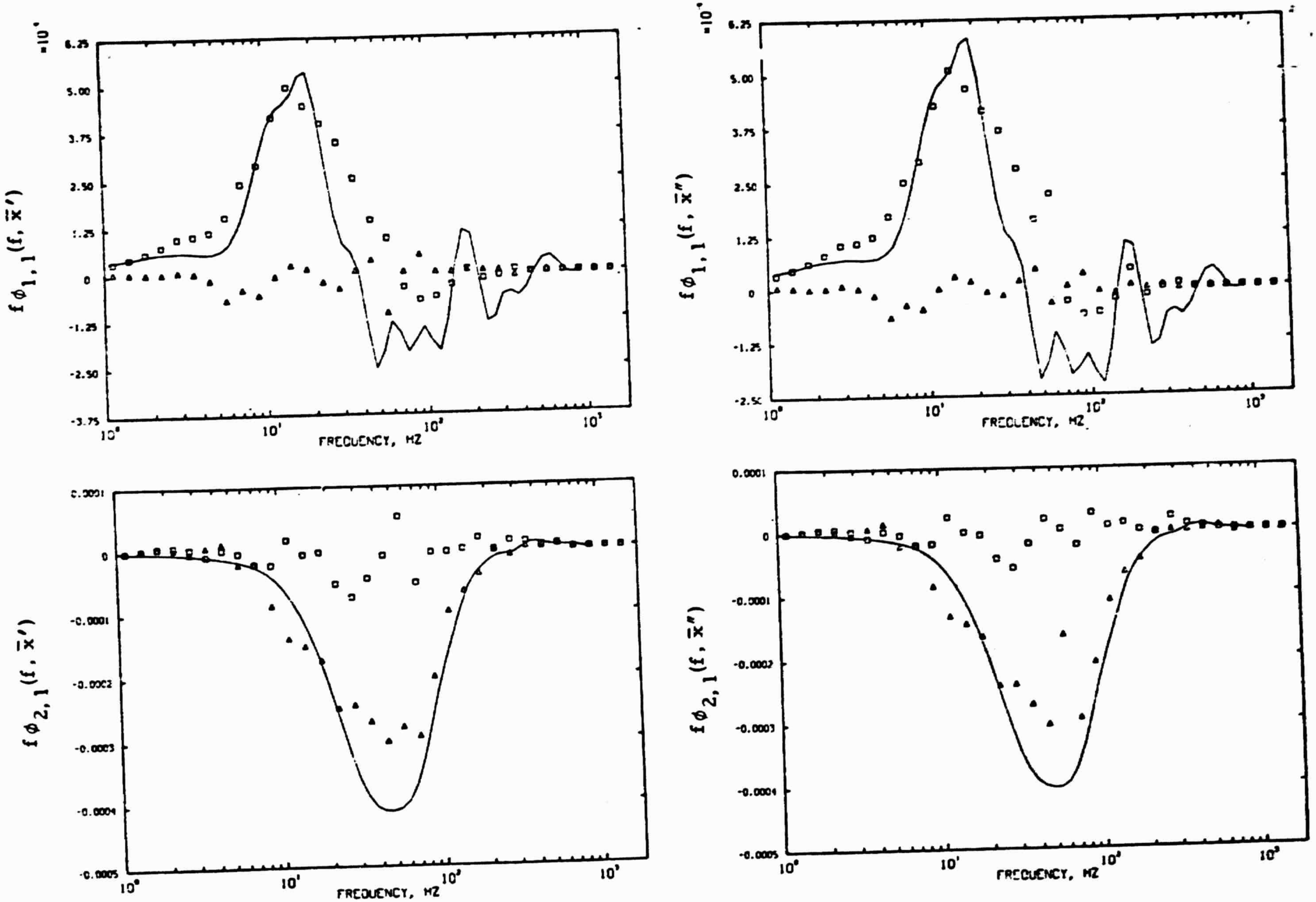

Fig. 11. Comparison of experimental and theoretical cross spectra for Case 8.4. □, Experimental real part; Δ, experimental imaginary part; ——— theoretical spectrum derived from autocorrelations of Fig. 5 using isotropy.

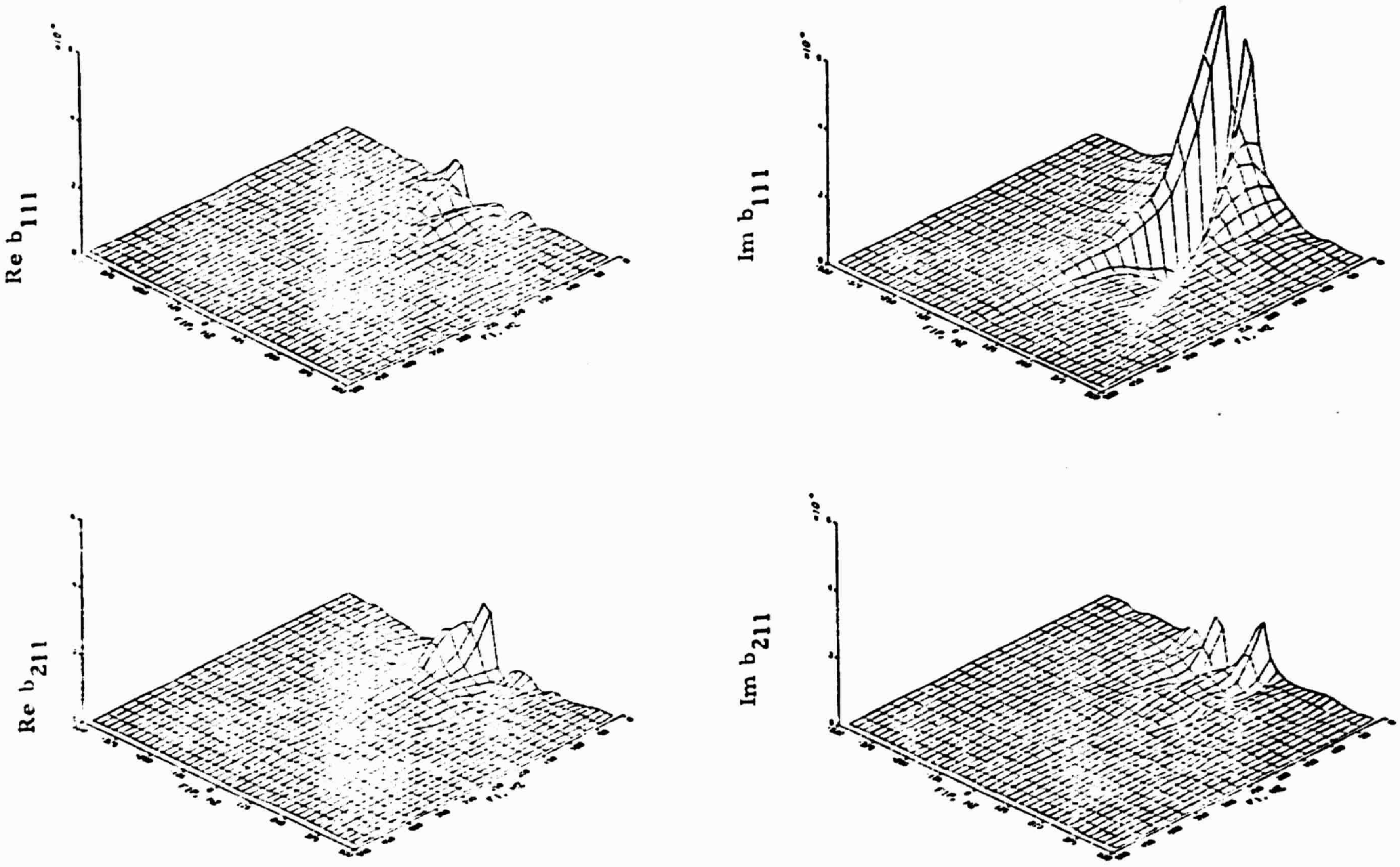

Fig. 12. One-dimensional bispectra $b_{111}(f, f'; \bar{x}, \bar{x}', \bar{x}'')$ and $b_{211}(f, f'; \bar{x}, \bar{x}', \bar{x}'')$ for Case 6.10.

ORIGINAL PAGE IS
OF POOR QUALITY

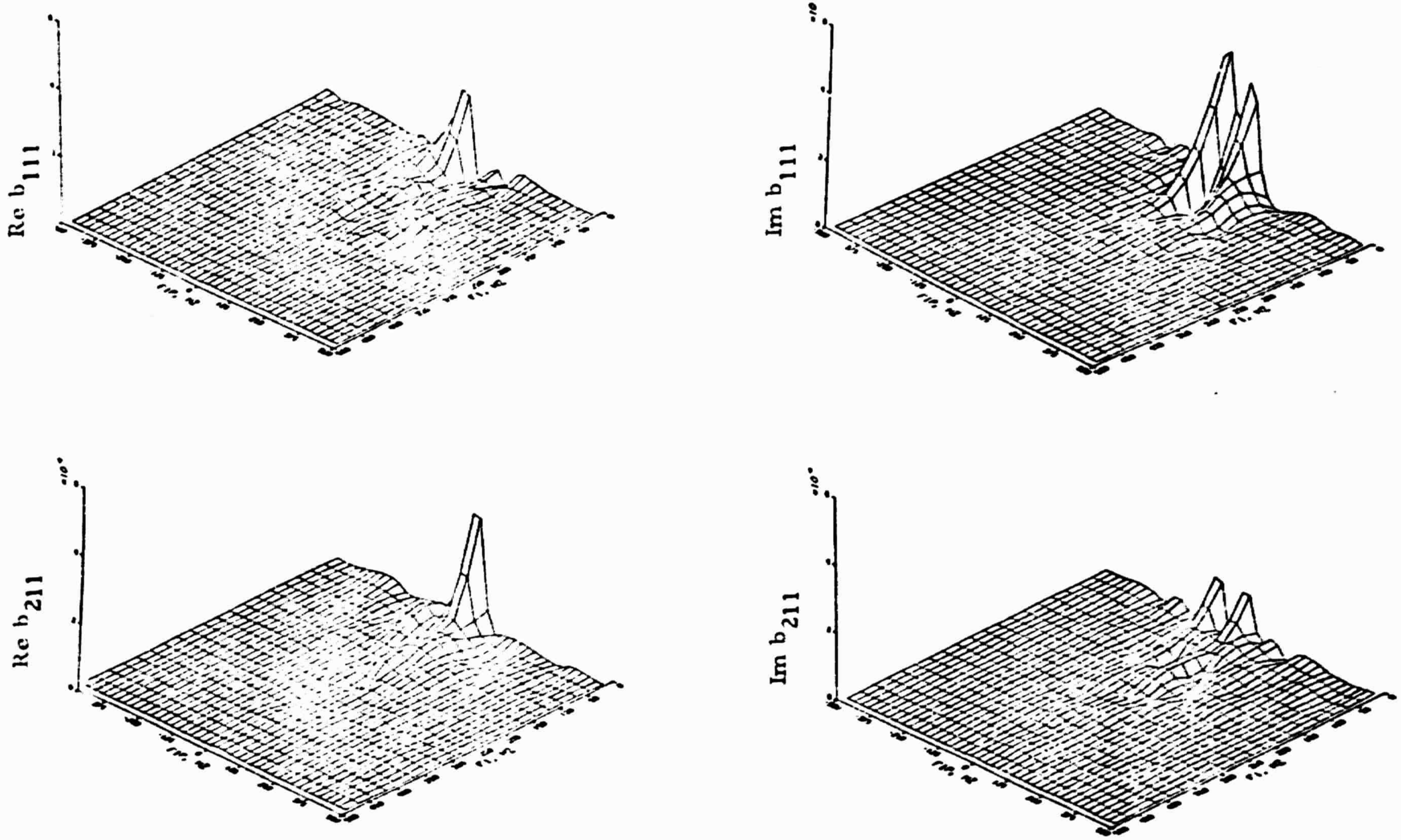

Fig. 13. One-dimensional bispectra $b_{111}(f, f'; \bar{x}, \bar{x}', \bar{x}'')$ and $b_{211}(f, f'; \bar{x}, \bar{x}', \bar{x}'')$ for Case 5. 2.

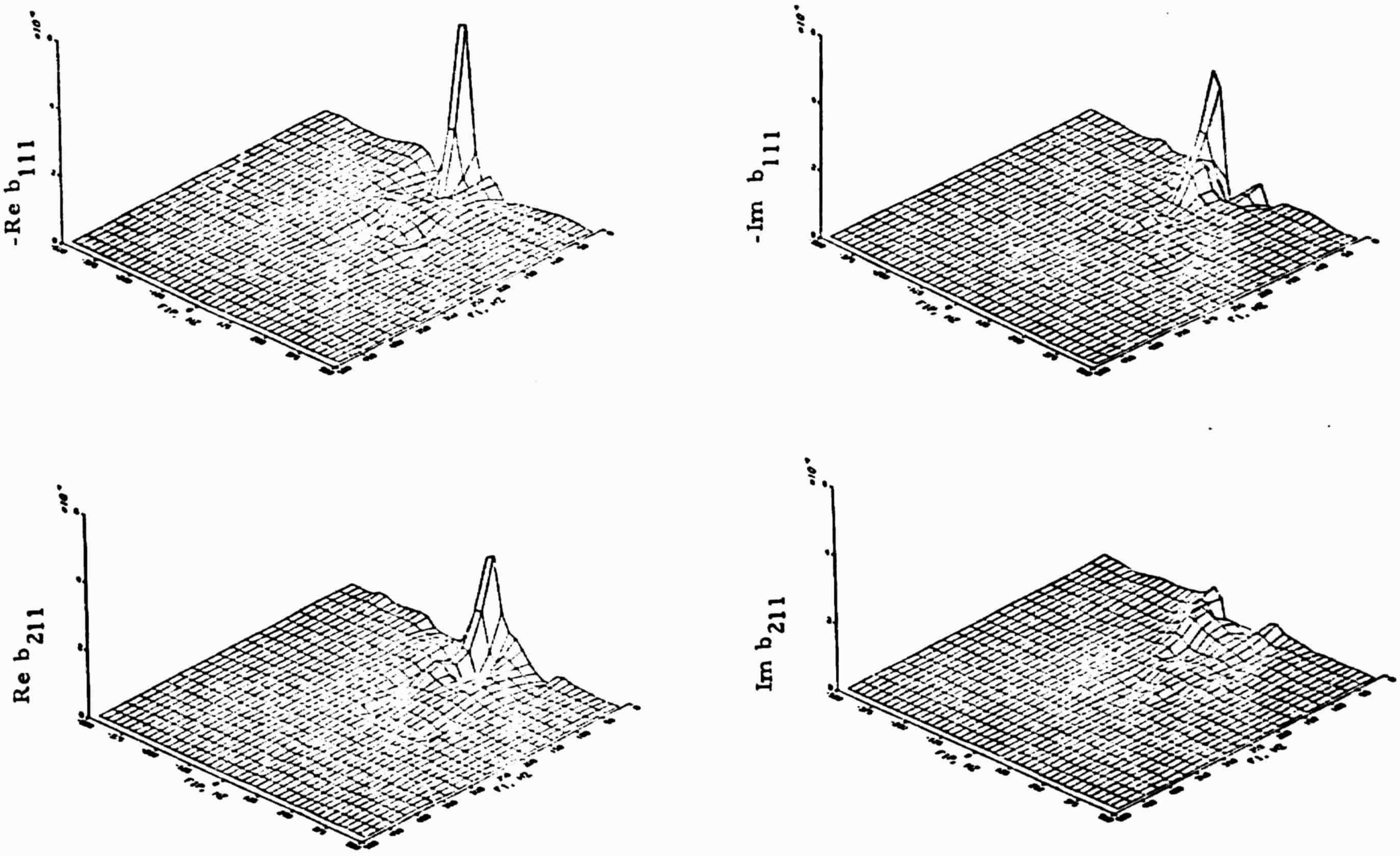

Fig. 14. One-dimensional bispectra $b_{111}(f, f'; \bar{x}, \bar{x}', \bar{x}'')$ and $b_{211}(f, f'; \bar{x}, \bar{x}', \bar{x}'')$ for Case 8.4.

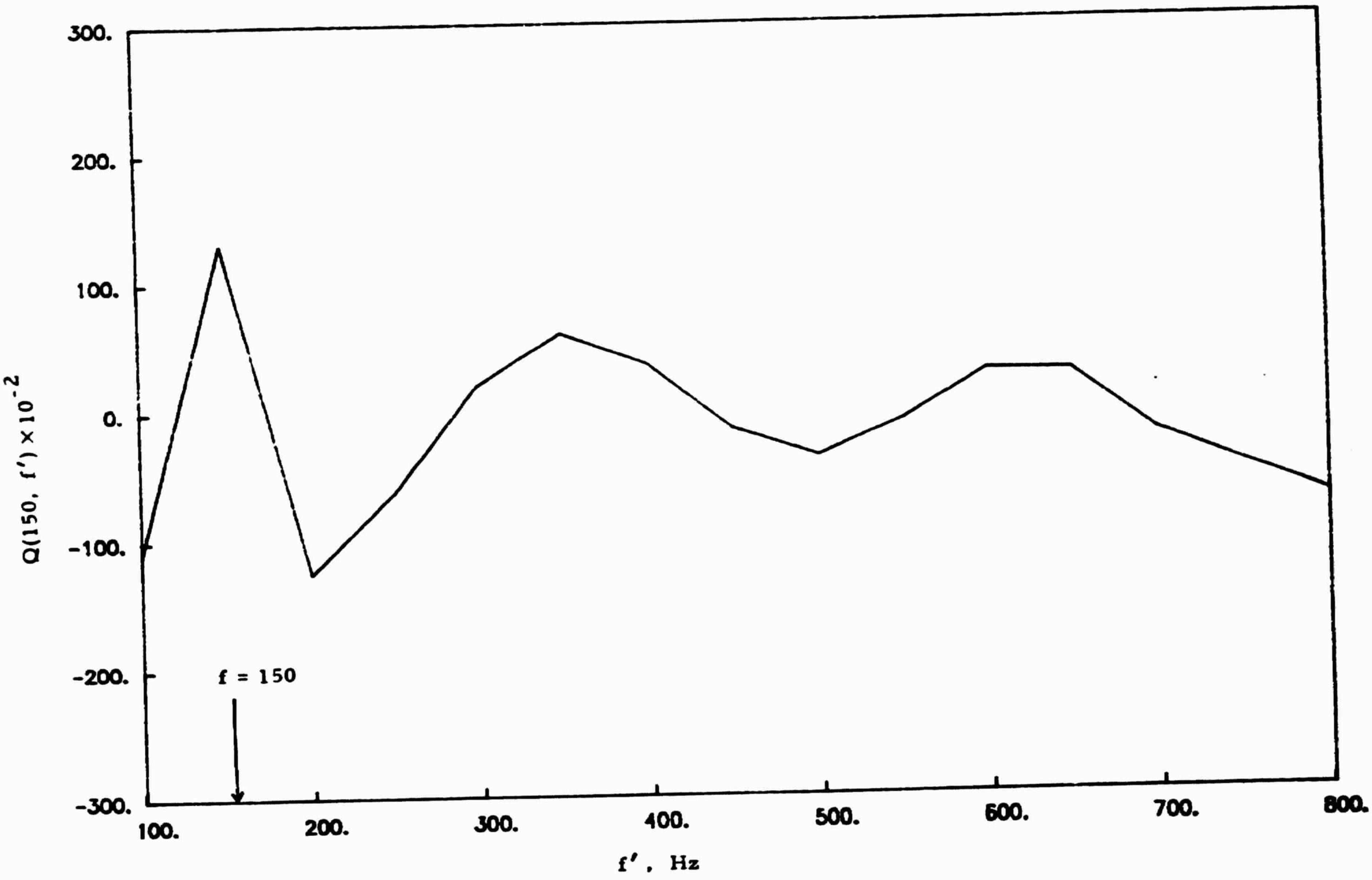

Fig. 15. Net three dimensional energy transfer from f' to $f = 150$ Hz.

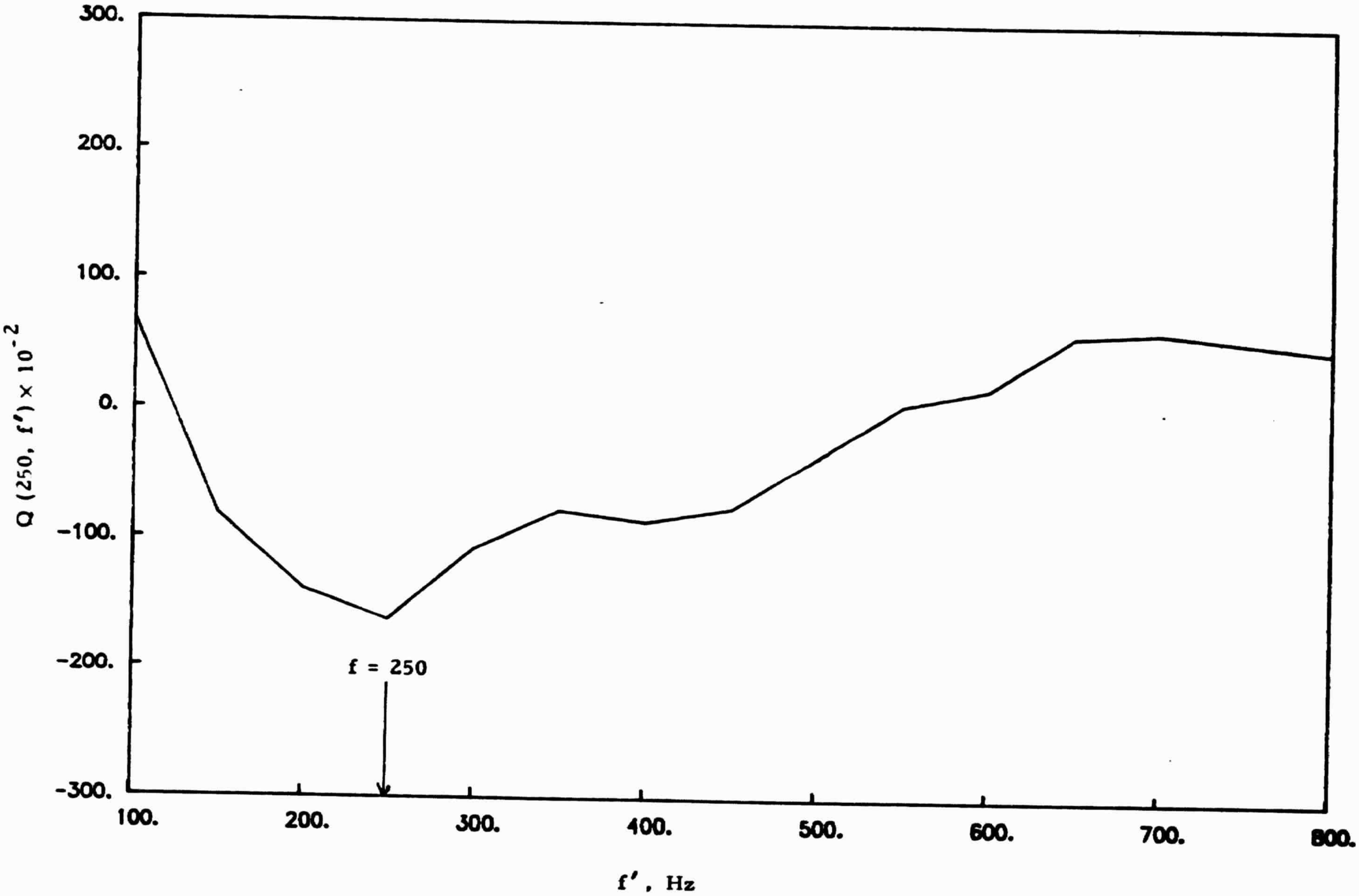

Fig. 16. Net three dimensional energy transfer from f′ to f = 250 Hz.

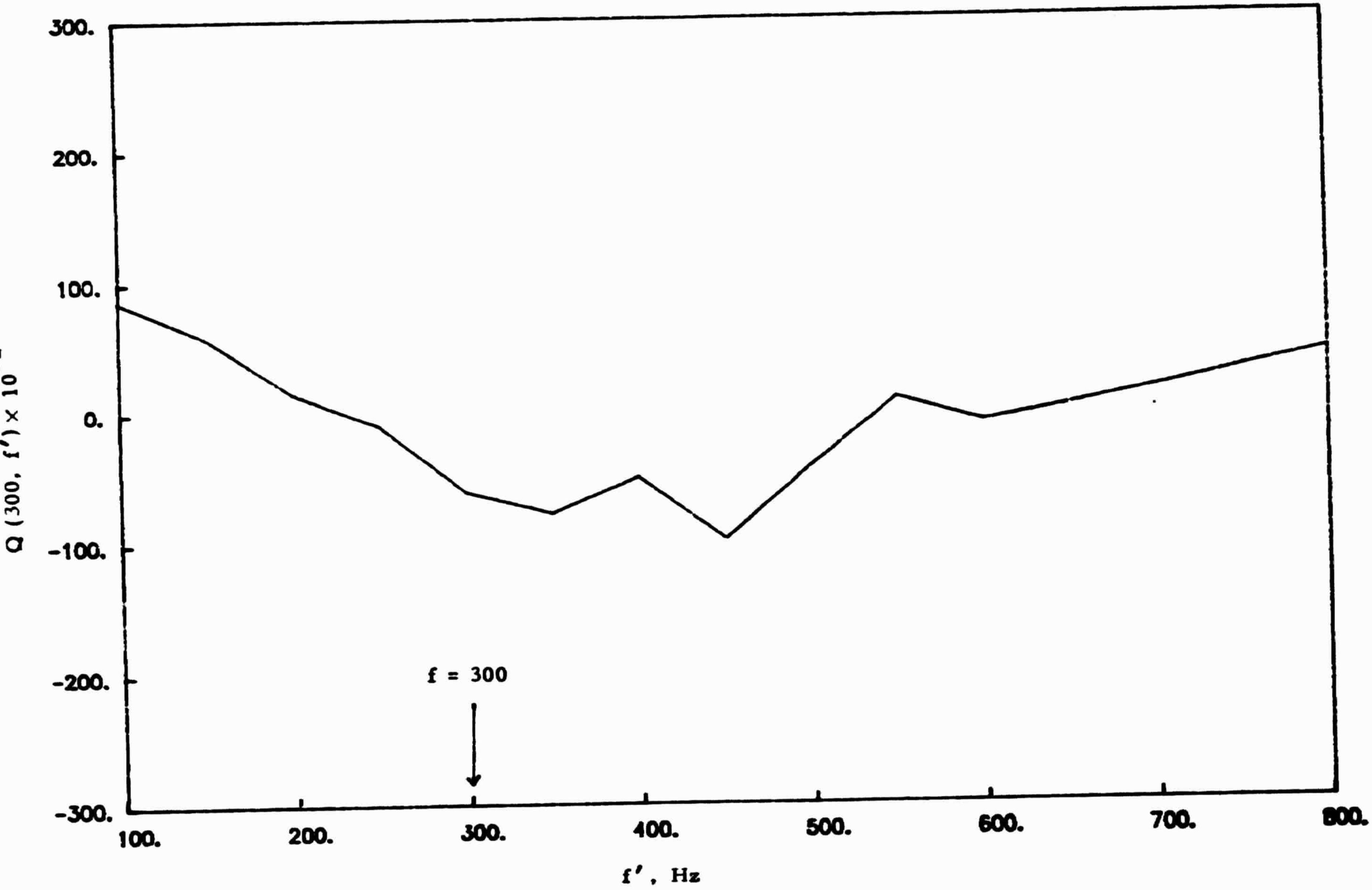

Fig. 17. Net three dimensional energy transfer from f′ to f = 300 Hz.

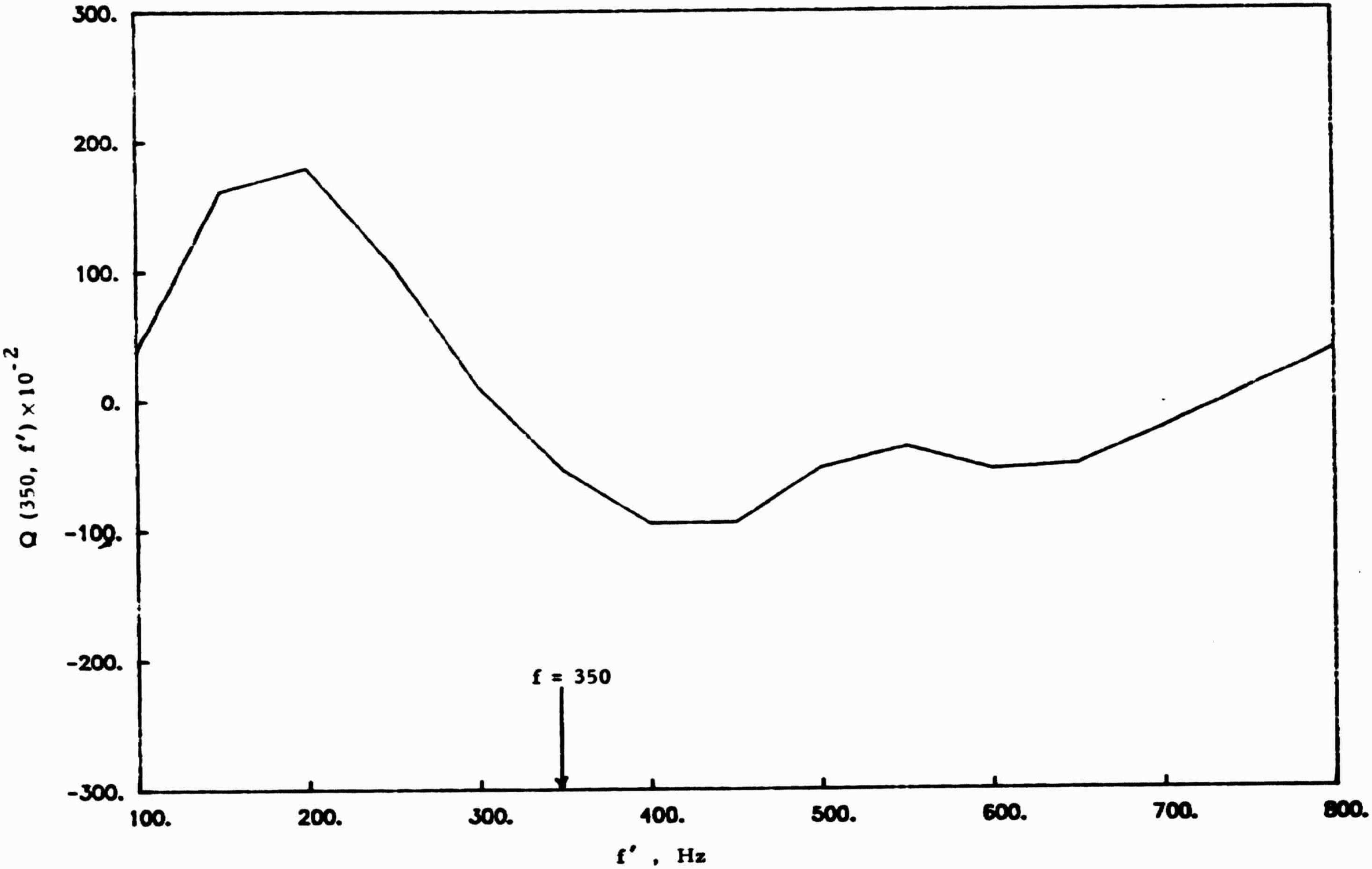

Fig. 18. Net three dimensional energy transfer from f′ to f = 350 Hz.

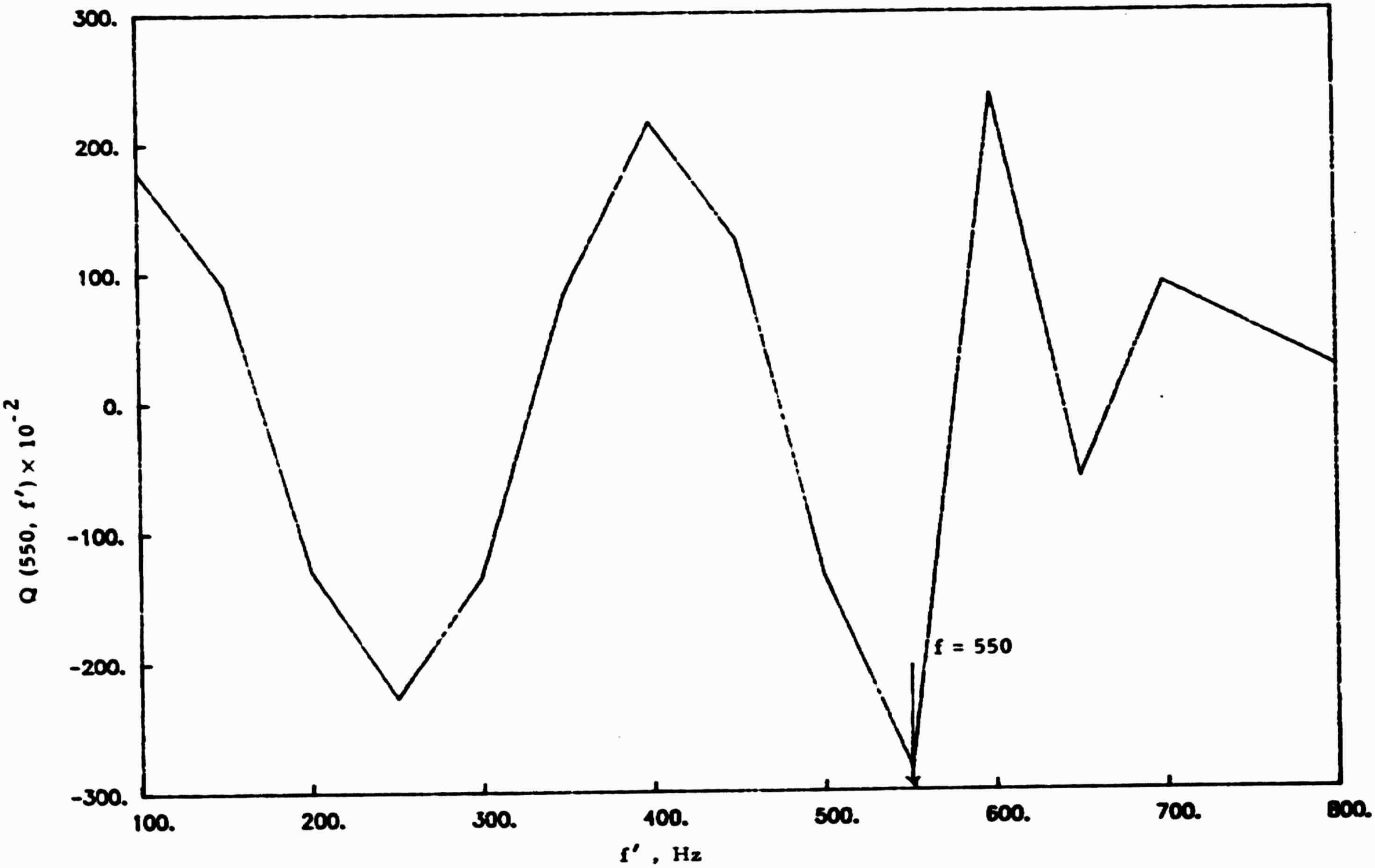

Fig. 19. Net three dimensional energy transfer from f' to f = 550 Hz.